Molecular aspects of electron correlation in quantum dots

2000 J. Phys.: Condens. Matter 12 R299

(http://iopscience.iop.org/0953-8984/12/22/201)

J. Phys.: Condens. Matter **12** (2000) R299–R334. Printed in the UK PII: S0953-8984(00)64921-4

REVIEW ARTICLE

Molecular aspects of electron correlation in quantum dots

P A Maksym†‡, H Imamura§, G P Mallon† and H Aoki‡

† Department of Physics and Astronomy, University of Leicester, University Road, Leicester LE1 7RH, UK

‡ Department of Physics, University of Tokyo, Hongo, Tokyo 113-0033, Japan

§ Graduate School of Information Sciences, Tohoku University, Sendai 980-8579, Japan

Received 1 March 2000

Abstract. The theory of electron correlation in semiconductor quantum dots is reviewed with emphasis on the physics of dots in strong magnetic fields. A brief survey of dot fabrication and experimental results is given, the quantum mechanics of small numbers of interacting electrons in a dot is discussed and the special values of angular momentum quantum number that the ground state is allowed to have, or magic numbers, are introduced. These numbers are selected because of the symmetry properties of the ground state and the symmetry is particularly evident in the limit of strong magnetic field if the system is examined in a moving reference frame. Physically, the system in this limit can be pictured as an electron molecule that rotates and vibrates in the dot, and this is the quantum dot analogue of a Wigner crystal. This is illustrated with a detailed treatment of a two-electron dot which can be studied without resorting to any special concepts of molecular physics. Next, the molecular physics concepts, such as the Eckart reference frame, needed to deal with rotational–vibrational motion of larger numbers of electrons are introduced. The physics of dots with more than two electrons is then described, including the evolution of magic numbers with electron number and the implications of symmetry. Finally, the extension of these ideas to larger systems and coupled dots is briefly discussed. Quantum dots in strong magnetic fields provide a unique opportunity to realize what could be called electron molecular physics, and some possible ways of probing the system experimentally are also proposed.

1. Introduction

Semiconductor quantum dots are nanostructures that can confine a few electrons in three dimensions. They are currently under intense study because they exhibit rich and elegant physics [1, 2] and have potential applications such as lasers and memory devices [3–6]. The importance of electron correlation in dots has been appreciated since the pioneering work of Bryant [7] who showed that ordered states should occur in dots with large electron spacing. These states are the few-electron analogue of a Wigner crystal and they have been called Wigner or electron molecules [8]. Similar states were found in a three-electron system during numerical studies of the fractional quantum Hall effect [9] and should generally occur in dots in a strong magnetic field [10]. These states have not yet been probed experimentally but advances in experimental technique could make them accessible soon and it seems timely to review their properties. This is the purpose of the present work which is a review of dot physics, with emphasis on electron molecular states in strong magnetic fields.

The electron molecular states should occur under similar conditions to those required for a Wigner crystal in a bulk system. The bulk Wigner crystal occurs in the low-electron-density limit [16], and the 2D Wigner crystal is particularly relevant because the vertical confinement in typical dots is much stronger than the lateral confinement. The quantum dot analogue of the 2D

0953-8984/00/220299+36$30.00

Wigner crystal is a large dot that contains a few electrons. The physics of this system has been explored in some detail [8, 11–14] for various dot geometries. It is believed that a transition from a liquid-like state to an ordered, molecular state occurs as the electron density decreases and the transition is predicted to occur at a surprisingly small electron separation [15]. Wigner crystallization in bulk 2D systems is enhanced by the application of a strong magnetic field in the perpendicular direction [16]; for example the 2D Wigner crystal is not observed in GaAs at zero field but does occur in the strong-field limit. The reason for this is that bulk single-electron states tend to be localized in the strong-field limit and this enhances the tendency to form ordered states when the electrons interact. Similarly, molecular states can occur in relatively small dots in the presence of a strong magnetic field. This could be advantageous for probing electron molecular states experimentally: a small dot is less likely to be affected by impurities than a large one.

The present work opens with a brief introduction to dots which covers the principles of dot fabrication and electron confinement, details the standard theoretical model of a dot and summarizes experimental techniques (section 2). The model has the electrons moving in two dimensions and confined laterally by a parabolic potential. This simple approach describes dot physics rather well and the reasons for this are also explained in section 2. The quantum mechanics of interacting electrons in a parabolic potential is described in section 3. First, the single-electron states are introduced and their properties are described, with emphasis on the way in which the angular momentum of the states and the magnetic field affect dot physics. Next, the quantum states of interacting electrons are discussed and the magic angular momentum quantum numbers are introduced. These are the only angular momenta the ground state can have and, as the magnetic field increases, the ground state undergoes a series of transitions in which its angular momentum goes through the sequence of magic values. The magic number sequence is characteristic of the electron number and total spin. As explained in section 3, the reason for this is a tendency for correlated electron states to centre on the classical minimum-energy configuration. As the magnetic field increases the quantum states become strongly localized about the classical minimum and the system can be pictured as an electron molecule.

This idea is developed quantitatively in the second part of this work. In contrast to a Wigner crystal, where the equilibrium positions of the electrons are fixed, the electron molecule both rotates and vibrates. It is not possible to separate the rotation and vibration completely but it is possible to find a reference frame in which the rotational–vibrational coupling is minimized. This frame is the Eckart frame that is normally used to study real molecules but the Eckart frame treatment of a many-electron dot is complicated by the need to deal with Coriolis forces and the need to construct anti-symmetric states from the rotational–vibrational states. However, two-electron molecular states can be treated without resorting to the Eckart frame and this is done in section 4 to introduce the electron molecular picture quantitatively and demonstrate that it is very accurate. The Eckart frame theory and the anti-symmetrization problem are then discussed in section 5 where it is shown that the low ground-state energy of the magic number states emerges naturally when Eckart frame rotational–vibrational states are anti-symmetrized.

The final part of this work is concerned with the physics of few-electron molecules (section 6). For up to six electrons, ground-state energies calculated within the molecular picture agree with exact-diagonalization results to better than 1% and excitation energies to a few per cent. For up to four electrons the physical picture of a state localized about the classical minimum works very well. But for larger numbers of electrons there are competing classical minima and this enriches the physics. For example, the six-electron system has both sixfold and fivefold correlation and there are selection rules that determine which form of correlation occurs in the ground state at a particular angular momentum. Thus molecular states can still

occur despite the existence of competing minima. However, there are special angular momenta at which both fivefold and sixfold correlation are allowed to occur. In this case the ground state can be thought of as a mixture of fivefold and sixfold states and its nature is 'liquid-like' rather than molecular. Remarkably, the mixing is only allowed to occur at the same odd-denominator Landau level filling factors where quantum Hall liquids occur in macroscopic systems and it is believed that similar mixing would occur in dots with more than six electrons. The physics of larger systems is considered in section 7 and this section also includes a discussion of the prospects for probing electron molecular states experimentally. An appendix details the treatment of the two-electron classical system which is closely related to the treatment of the two-electron quantum system.

Throughout this work the physics is illustrated with the authors' numerical results for GaAs dots (effective mass: $m^* = 0.067m_0$ with m_0 the free-electron mass; dielectric constant: $\epsilon = 12.4$; effective g-factor: $g^* = -0.44$). Some of the results have not been published elsewhere.

2. Quantum dots

Semiconductor quantum dots are generally fabricated by applying a lateral confining potential to a two-dimensional electron system [1, 2]. A modulation-doped quantum well or heterojunction is first grown to provide strong electron confinement in the growth direction, then nano-fabrication techniques are used to obtain the lateral confinement. The simplest technique is mesa etching, which results in a free-standing quantum dot [17], but an electrostatic confining potential [18] is used to make the majority of dots. A popular approach is to deposit an insulating cap above a two-dimensional system and cover the whole structure with a metallic gate. When a negative bias is applied to the gate, a small number of electrons, say 1–100, can be confined underneath the cap (figure 1, left-hand side). More recently, very high-quality dots have been fabricated by a combination of mesa etching and electrostatic confinement in which a metallic gate is deposited around a mesa-etched pillar [19] (figure 1, right-hand side). A number of alternative lateral-confinement techniques are also used, such as systems of gates used without a cap [20] and stressors deposited on the semiconductor surface [21]. In addition, there have been proposals to confine electrons by spatially modulated magnetic fields [22–24] and dots can be fabricated directly by self-organized growth [25].

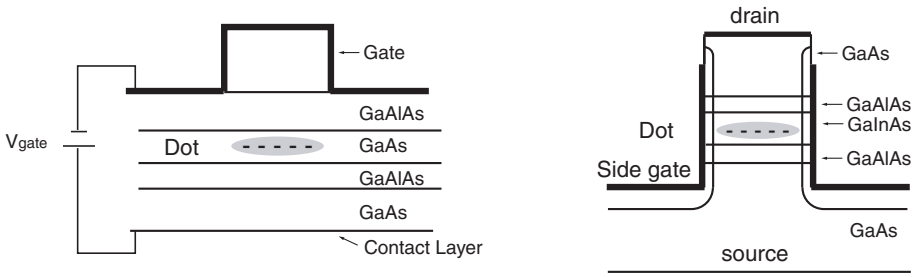

Figure 1. Schematic illustrations of typical electrostatic quantum dots. Left-hand side: capped dot; right-hand side: pillar dot. The capped dot can be made either from a quantum well (as shown) or from a heterojunction.

This review is particularly concerned with electrostatic dots which are defined by a cylindrical pillar or a cap of square or circular shape. The lateral-confinement scale in these dots is typically 50–100 nm, the associated confinement energy scale is around 2–4 meV and

several groups have fabricated dots that can confine a few electrons or even just one electron. The standard theoretical model of these systems is based on a number of approximations. First, the electron motion is taken to be exactly two dimensional. This is reasonable because a typical dot is constructed from a quasi-two-dimensional system in which the sub-band energy spacing is large compared to the thermal energy k_BT. Secondly, the potential is taken to be cylindrically symmetric. This is always true for cylindrical dots and dots with circular caps but it is also a good approximation for dots with square caps, for example those used for optical studies [17]. This is because the confinement length is typically much smaller than the cap size so the cap has only a small influence on the symmetry of the potential deep inside the dot where the wave function is large. The third approximation is that the confining potential is parabolic. This is again reasonable because a fairly large voltage, typically -1 V, is applied to the gate. Thus the electrons are confined in a potential well whose depth is around 1 eV, large compared to the typical energy scale. This means that the electron wave function is only large close to the minimum of the well where the potential is parabolic. The final approximation is that the electrons interact via a pure Coulomb interaction. In a real dot the electron–electron interaction is usually screened (see the next paragraph) but the Coulomb approximation generally explains the physics. Within the standard theoretical model, the Hamiltonian for electrons interacting in a dot in a magnetic field, B, perpendicular to the dot plane is

$$H = \sum_{i=1}^{N}\left[\frac{1}{2m^*}\Big(\boldsymbol{p}_i + e\boldsymbol{A}(\boldsymbol{r}_i)\Big)^2 + \frac{1}{2}m^*\omega_0^2 r_i^2\right] + \frac{1}{2}\left(\frac{e^2}{4\pi\epsilon\epsilon_0}\right)\sum_{i=1}^{N}\sum_{\substack{j=1\\ j\neq i}}^{N}\frac{1}{|\boldsymbol{r}_i - \boldsymbol{r}_j|} + g^*\mu_B B S_z \qquad (1)$$

where the first term is the one-electron term, the second term is the Coulomb interaction term and the last term is the Zeeman energy. The z-component of the total spin is S_z, m^* is the effective mass, g^* is the effective g-factor, ϵ is the dielectric constant and $\hbar\omega_0$ is the confinement energy. The system is axially symmetric, so it is convenient to use the symmetric gauge, and the magnetic vector potential is $\boldsymbol{A} = (B/2)(\hat{\boldsymbol{k}}\times\boldsymbol{r})$, where $\boldsymbol{r}$ is a position vector in the dot (x, y) plane and $\hat{\boldsymbol{k}}$ is a unit vector in the z-direction. Dots of lower symmetry can be fabricated [26] and studied theoretically with a model similar to the one described here [27–29].

The standard theoretical model is believed to account for the general physics of dots but modifications of the confinement and interaction potentials probably need to be considered to understand experimental data in fine detail [30–32]. The best evidence for the validity of the model is that far-infra-red (FIR) absorption spectra are found to be almost independent of the number of electrons in a dot [17, 18, 33, 34]. This is a consequence of the generalized Kohn theorem [35, 36]. Essentially, FIR radiation, whose wavelength is much larger than the dot size, can only affect the motion of the centre of mass of the electrons, but in a parabolic confining potential the centre-of-mass (CM) and relative (RM) motion decouple. Thus only CM excitations can be observed in a FIR experiment and their energy depends only on the charge-to-mass ratio of the CM so is independent of the electron number. The observed excitation energies have some small splittings which have been attributed to small deviations from parabolic confinement [37, 38]. It is also possible that small deviations from 2D motion could affect FIR spectra, particularly in devices with a small sub-band gap [32]. There is less experimental information about the form of the interaction potential in real dots but it is likely that there are screening effects caused by the metallic gates used to define the dot. This makes the interaction dipole-like at long range [39, 40] and in addition the effective interaction at short range is affected by the finite extent of the wave function in the growth direction [31, 32].

Experimental studies of dots involve optical spectroscopy, transport measurements and investigations of dot charging. The first optical studies were concerned with FIR absorption spectroscopy of dot arrays but spectroscopy of single dots is now possible [41] and there

is increasing interest in Raman spectroscopy [42]. Transport and charging studies make use of the Coulomb blockade to control tunnelling of electrons into and out of a dot [43]. In the simplest case, dots used for these studies resemble those shown in figure 1. The dot is coupled to an electron source whose electrochemical potential is μ_S and a drain whose electrochemical potential is μ_D. The electrochemical potential of the N-electron dot $\mu(N+1, V)$ depends on both the electron number and the gate voltage V and, at zero temperature, $\mu(N+1, V) = E_0(N+1, V) - E_0(N, V)$ where $E_0(N, V)$ is the ground-state energy. In this non-equilibrium situation, electron tunnelling into and out of the dot is impeded unless $\mu_S \geqslant \mu(N+1, V) \geqslant \mu_D$. This resonance condition can be set for different values of N by changing the voltage of the gate, so peaks occur in the dot conductance as a function of gate voltage [19, 20, 44–50]. Dots with more than one gate electrode can also be made and in this case each gate voltage can affect transport through the dot. As an alternative to transport, an elegant way of probing the resonance condition is to use an integrated dot and electrometer to measure the charge in the dot directly [51, 52]. Transport and charging studies have become quite sophisticated and recent developments include the study of photon-assisted single-electron tunnelling [53, 54] and evidence for charge redistribution associated with changes in the electronic state of a dot [55].

The experimental studies done to date have provided convincing evidence that single electrons can be confined and manipulated in quantum dots. In addition, the observed physics is in agreement with the predictions of the 2D parabolic model, although a detailed analysis of experimental data for a specific device, including corrections to the confinement and interaction potentials, remains to be done. Further details can be found in various reviews [34, 43, 56–60] and texts [1, 2]. In contrast, the high-field regime described here should contain rich and unexplored physics that is challenging to study experimentally.

3. Quantum mechanics of electrons in a dot

3.1. Single-electron states

The eigenstates of non-interacting electrons in a 2D parabolic potential were first investigated by Fock [61] and Darwin [62] in early studies of diamagnetism. In the quantum dot literature these states are known as the Fock–Darwin states and they have the form

$$\psi_{nl}(\boldsymbol{r}) = \frac{1}{\sqrt{2\pi\lambda^2}}\left[\frac{n!}{(n+|l|)!}\right]^{1/2}\left(\frac{r}{\sqrt{2}\lambda}\right)^{|l|} L_n^{|l|}(r^2/2\lambda^2)\exp(-r^2/4\lambda^2)\exp(-\mathrm{i}l\phi) \tag{2}$$

with energies given by

$$E_{nl} = (2n+1+|l|)\hbar\Omega - l\hbar\omega_c/2 \tag{3}$$

(excluding the Zeeman energy). Here l and n, respectively, are angular momentum and radial quantum numbers, $L_n^{|l|}$ is an associated Laguerre polynomial, $\Omega^2 = \omega_0^2 + \omega_c^2/4$ and $\omega_c = eB/m^*$ is the cyclotron frequency. The length parameter, λ, given by $\lambda^2 = \hbar/(2m^*\Omega)$ sets the overall length scale. This parameter depends on the magnetic field so the Fock–Darwin states become the states of a 2D harmonic oscillator in the zero-field limit and the Landau states of a free electron in the ultra-strong-field limit. Physically, the states are localized on rings of width $\sim\lambda$, with a radius, R, dependent on the quantum numbers l and n and also on λ. Strictly speaking, R is determined by the position of the maxima of $|\psi_{nl}|^2$ but a good approximation is to take R^2 to be the mean square radius of ψ_{nl}. Thus

$$R^2 = \langle n, l|r^2|n, l\rangle = 2\lambda^2(2n+|l|+1) \tag{4}$$

and R increases with angular momentum. In addition, the radius *decreases* with magnetic field because λ approaches the cyclotron length, $\sqrt{\hbar/(eB)}$, in the strong-field limit.

Dot physics is strongly influenced by the magnetic field and angular momentum dependence of the Fock–Darwin states. For example, the Fock–Darwin energies as a function of field are shown in figure 2 for a GaAs dot with $\hbar\omega_0 = 2$ meV. Typically, the energies first decrease with field and then increase linearly in the asymptotic field regime. The initial decrease reflects the compression of the wave function induced by the magnetic field, which forces the wave function to exist in a region of lower potential energy. As the field increases further, the zero-point energy of the cyclotron motion becomes dominant and the levels coalesce into Landau levels of energy $(N_L + 1/2)\hbar\omega_c$, where the Landau quantum number $N_L = n + (|l| - l)/2$. However, when the field is finite but strong, each Landau level in a dot is broadened and the states with larger l have larger energy because they have a larger radius and hence exist in a region of larger potential.

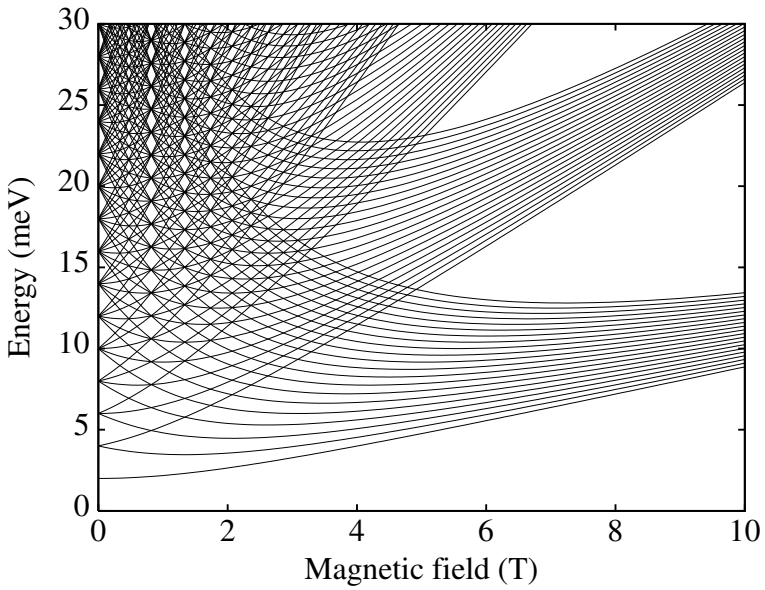

Figure 2. Fock–Darwin energy levels as a function of magnetic field for $\hbar\omega_0 = 2$ meV. The levels shown are the lowest 200 at $B = 0$ T.

3.2. Interacting electron states

Electron correlation in dots has been studied with various methods, and exact diagonalization of the few-electron Hamiltonian has been particularly reliable and informative. Small 2D systems in a magnetic field with [9] and without [63] a confining potential were first investigated during early studies of the fractional quantum Hall effect. Subsequently, Bryant [7] pioneered exact-diagonalization studies of electrons interacting in quantum boxes and then Maksym and Chakraborty [36] investigated interactions in a 2D parabolic dot in a perpendicular magnetic field. Other methods for studying correlation enable larger electron numbers to be treated than is possible with exact diagonalization, at the expense of making some approximations whose validity is not always clear. For example, the Hartree–Fock method [64–66] has been used for dots in zero and non-zero magnetic field and the density functional method [67] has been used to study dots in zero magnetic field. Current density functional theory [68] is a

promising approach to studying large interacting systems in the presence of a magnetic field. Finally, an alternative to numerical studies is to find special interaction potentials for which the Schrödinger equation is analytically soluble [57].

The magnetic field dependence of the ground-state energy is particularly interesting and relevant to dot physics. For example, results obtained by exact diagonalization are shown in figure 3 for the case of three spin-polarized interacting electrons and $\hbar\omega_0 = 2$ meV. The figure shows both the total ground-state energy (solid line) and its decomposition into one-electron, Coulomb and Zeeman components which was obtained by taking the ground-state expectation value of the corresponding terms in equation (1). While the total energy is almost smooth on the scale of the figure, the one-electron and Coulomb components change discontinuously. These discontinuities reflect the influence of the magnetic field on the extent of the wave function. The increasing field reduces the system size and hence increases the Coulomb energy. Just as in the one-electron case (equation (4)), the system can expand by increasing

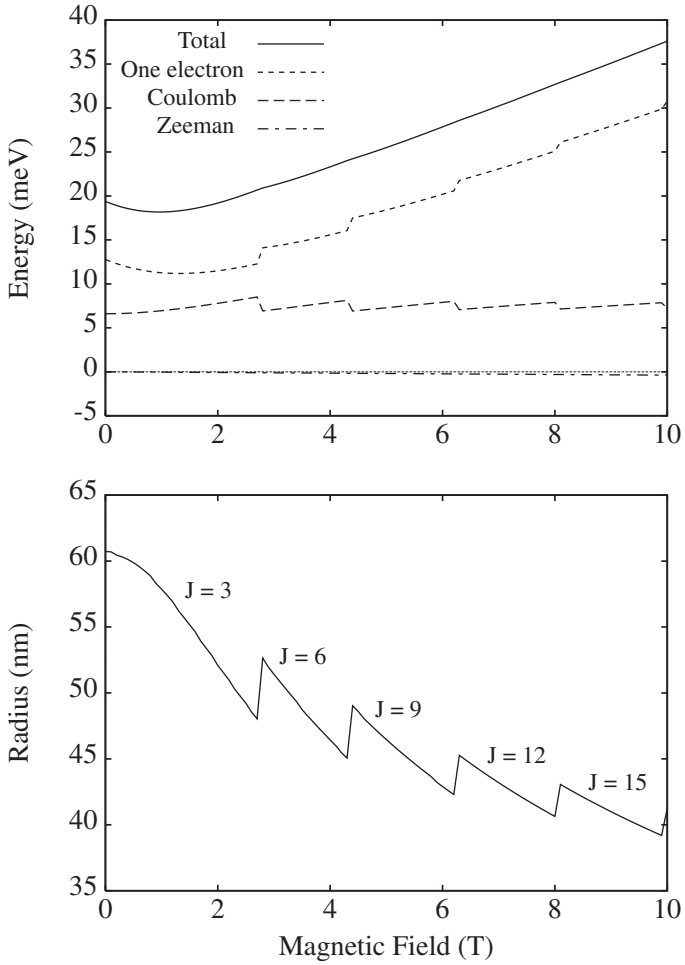

Figure 3. Ground-state properties as a function of magnetic field for three spin-polarized electrons with $\hbar\omega_0 = 2$ meV. Upper frame: ground-state energy together with one-electron, Coulomb and Zeeman contributions; lower frame: effective dot radius obtained by numerically integrating the electron density.

the total-angular-momentum quantum number, J. This decreases the Coulomb energy but only happens at certain critical magnetic fields where the decrease in Coulomb energy can compensate for the increase of one-electron energy that results from the increase in J. The cycle repeats with increasing B and this leads to the oscillations shown in the figure. The abrupt changes in the orbital angular momentum are accompanied by abrupt changes in the system size (figure 3, lower frame). A convenient measure of the size is the radius of the circle, R_{eff}, that contains 95% of the charge. This is given by the solution of the equation

$$2\pi \int_0^{R_{eff}} n_e(r) r \, \mathrm{d}r = 0.95N$$

where $n_e(r)$ is the electron density [39]. Abrupt increases in R_{eff} clearly coincide with a transition to a new ground state. The increase of angular momentum with magnetic field is essentially a classical effect while the abruptness of the change in R_{eff} is a quantum mechanical effect which derives from angular momentum quantization (see section 4 and the appendix). Abrupt changes in dot size are also predicted by an approximate treatment due to Chamon and Wen [69] and it is likely that the effect has been seen in recent experimental work [55].

The magnetic field dependence of the ground-state energy in figure 3 is typical for electrostatic quantum dots containing small numbers of electrons. Extensive numerical studies have shown that angular momentum transitions always occur and in addition there are transitions in the total spin [70, 71]. The transitions are predicted to cause oscillations in thermodynamic properties of dots such as the electronic heat capacity [36] and magnetization [70, 71]. In addition, there is theoretical evidence that they affect transport [72, 73], luminescence [74] and optical [37, 75–77] properties of dots and influence the chemical potential [66, 78, 79]. It is likely that some of the transitions have been observed [52, 78].

3.3. Magic numbers

One of the most interesting aspects of correlated ground states in dots, and one that is particularly relevant to the present work, is that only certain combinations of the total orbital angular momentum and total spin are allowed to occur. For example, the ground-state angular momentum of three spin-polarized electrons is always a multiple of 3. The total energy of this system as a function of angular momentum (excluding the small Zeeman term) is shown in figure 4. Each point gives the lowest energy at a particular J-value and it is convenient to call the corresponding state 'a ground state'. The state of lowest total energy, which corresponds to the global minimum of the ground-state energy as a function of J, will be called 'the absolute ground state' or just 'the ground state' when the meaning of this term is clear. The two frames in figure 4 show the total energy at field points on either side of the transition from $J = 6$ to $J = 9$ in figure 3. In each case, the one-electron contribution increases almost linearly with J while the Coulomb contribution decreases, roughly like $1/\sqrt{J}$. Thus the total energy as a function of J has a minimum. As the magnetic field increases, compression of the wave function induced by the magnetic field drives the minimum to higher J (compare the top and bottom frames) and this is consistent with the physical arguments given in section 3.2. However, the total energy actually has the form of some subsidiary minima superimposed on a broad minimum and the global minimum always coincides with one of the subsidiary minima (see the arrows in figure 4). These minima have period 3 and the angular momentum of the absolute ground state is always a multiple of 3 for three spin-polarized electrons. In general, the absolute-ground-state angular momentum depends on both the electron number and the spin quantum number, S, that gives the total spin, $\boldsymbol{S}^2 = S(S+1)$, but is independent of the z-component of the spin, S_z. For instance, the absolute-ground-state J-value of the four-electron

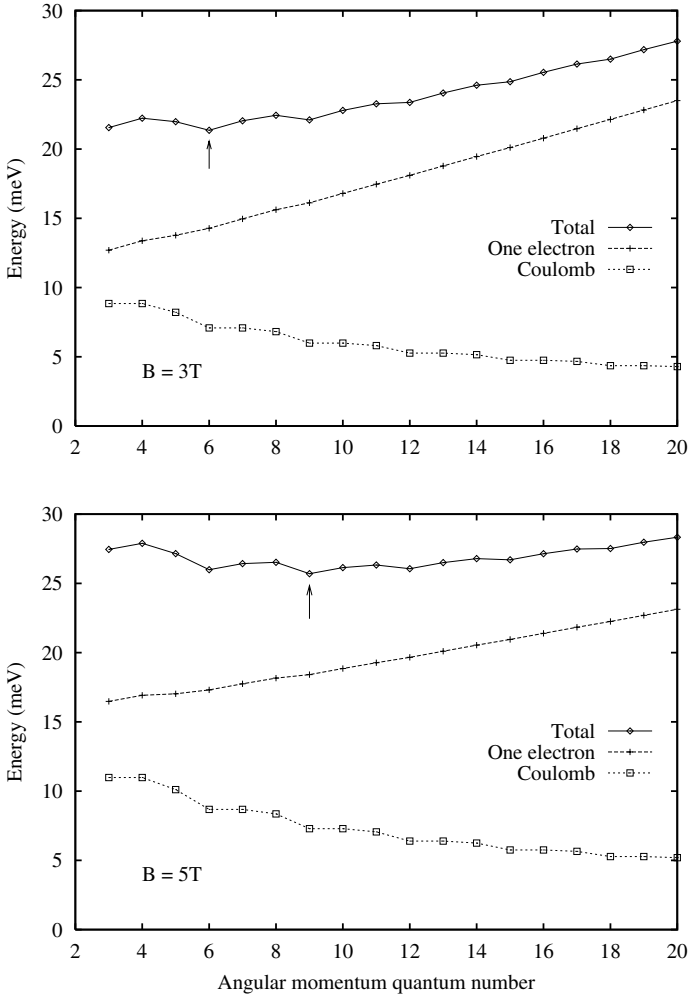

Figure 4. Energy as a function of total angular momentum for three spin-polarized electrons with $\hbar\omega_0 = 2$ meV. The one-electron energy, the Coulomb energy and the sum of these energies are shown. The points give the lowest energy for each value of total angular momentum. The lines are to guide the eye. The arrows indicate the minimum total energy.

system satisfies $J \equiv 2 \bmod 4$ when the system is spin polarized ($S = 2$) and $J \equiv 0 \bmod 2$ when the system is spin unpolarized ($S = 0$). The allowed absolute-ground-state angular momenta are known as the magic angular momentum numbers and investigations of why the absolute-ground-state angular momentum is restricted to one of the magic values have led to some very interesting physics.

The earliest approach to explaining the origin of the magic numbers was an argument based on exchange energy [70]. In the high-field limit, where Landau level mixing is negligible, the ground state is made up of Slater determinants for the zeroth Landau level. For spin-polarized electrons the Slater determinant for the zeroth Landau level that has the largest exchange energy is the one where all the electrons are adjacent in angular momentum space. This configuration can only occur at certain values of the total angular momentum and they are generally magic ones. For example, in the three-electron case one way of making the l-values adjacent is to

choose $l = 1, 2, 3$ which gives $J = 6$, one of the magic numbers of the three-electron system. The argument is similar to Hund's first rule in that the state of lowest total energy is the one where exchange effects are the largest. For larger numbers of electrons the large exchange energy that occurs when all the electrons are adjacent does not compensate for the larger Hartree energy and in this case the favourable configurations have $N - 1$ adjacent electrons with one electron in an $l = 0$ state. For example, $l = 0, 4, 5, 6, 7, 8$ gives $J = 30$, one of the magic numbers for six spin-polarized electrons. Numerical calculations show that these special configurations tend to occur in the ground state with high probability.

In more recent approaches symmetry has been used to connect favourable electron correlation with particular angular momentum values. The classical minimum-energy configuration of a few point charges in a parabolic potential is highly symmetric. For example, the minimum-energy configuration of three classical point charges is an equilateral triangle, or a rotating equilateral triangle if the system has non-zero angular momentum. It is reasonable to suppose that the quantum ground state is localized around the classical minimum but this is only compatible with the Pauli principle when the angular momentum is magic. In other words, the magic angular momenta are the only ones for which an anti-symmetric state is allowed to have correlations with the same symmetry as the classical energy minimum.

To determine the magic numbers it is necessary to find the angular momenta at which particular forms of correlation are allowed to occur. In early work on the three-electron spin-polarized system this was done by constructing a system of coordinates in which cyclic permutations and rotations are equivalent [10, 74]. Using these coordinates it is possible to show [10] that anti-symmetric ground states can only have maxima with threefold symmetry when the total angular momentum is a multiple of 3. A simpler argument, but one that only gives a sufficient condition, is to consider the wave function for special values of the electron coordinates [80]. For instance, consider the three-electron state $\Psi(\boldsymbol{r}_1, \boldsymbol{r}_2, \boldsymbol{r}_3)$ when $\boldsymbol{r}_1, \boldsymbol{r}_2, \boldsymbol{r}_3$ in cyclic order form the corners of an equilateral triangle. Ψ is invariant under cyclic permutations because they have even parity. But a cyclic permutation is equivalent to a $2\pi/3$ rotation under which Ψ becomes $\exp(2\pi \mathrm{i} J/3)\Psi$. This is only compatible with the invariance of Ψ when J is a multiple of 3, one of the magic numbers of the three-electron spin-polarized system. The argument can be generalized to arbitrary electron numbers and spins [80–82].

The link between magic numbers and the symmetry of the classical minimum is best verified by computing the pair correlation function [10, 81, 83, 84]. Axially symmetric quantities, such as the electron density, are unsuitable for visualizing angular correlations. In contrast, the pair correlation function has clear structure which gives insight into the physics. The pair correlation function is proportional to the probability of finding an electron at position $\boldsymbol{r}$, given that there is one at position $\boldsymbol{r}_0$. Mathematically, it is given by

$$P(\boldsymbol{r}, \boldsymbol{r}_0) = \frac{(2\pi\lambda^2)^2}{N(N-1)} \left\langle \sum_{i \neq j} \delta(\boldsymbol{r}_i - \boldsymbol{r}) \delta(\boldsymbol{r}_j - \boldsymbol{r}_0) \right\rangle \tag{5}$$

where the angled brackets denote an expectation value in a particular quantum state, usually the ground state. The term 'pair correlation function', used here to refer to $P(\boldsymbol{r}, \boldsymbol{r}_0)$, has been used elsewhere in the quantum dot literature but there seems to be no consistent terminology throughout the physics literature; for example the term 'two-particle correlation function' is also used to mean the same function. Figure 5 shows pair correlation functions for various states of three to six spin-polarized interacting electrons in a dot with $\hbar\omega_0 = 4$ meV. In each case the black spot indicates $\boldsymbol{r}_0$ and r_0 coincides with the maximum electron density. Part (a) of the figure shows how the ground-state pair correlation functions of the three-electron system depend on magnetic field. At zero field the pair correlation function has a crescent-shaped maximum opposite the fixed electron but at higher fields it has two peaks and these

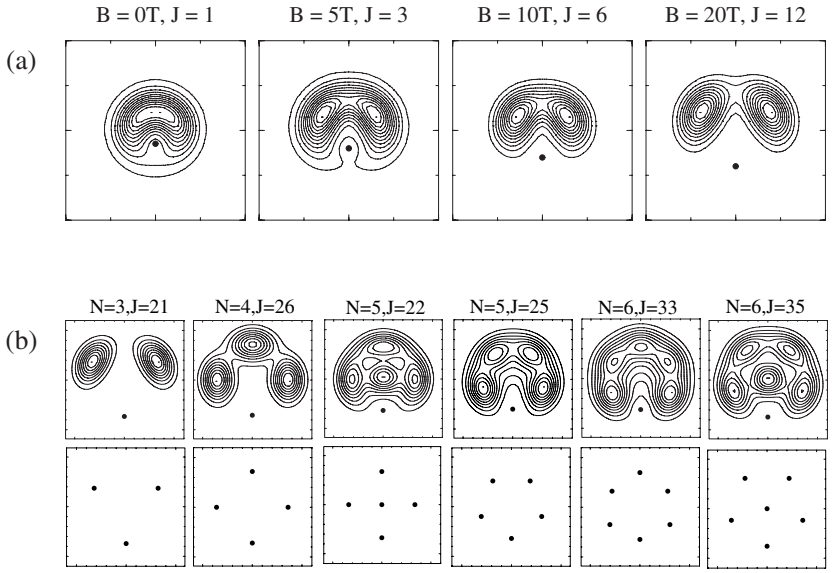

Figure 5. (a) Ground-state pair correlation functions at selected field points for three interacting electrons with $\hbar\omega_0 = 4$ meV. The total spin is $1/2$ at $B = 0$ T and $3/2$ at higher fields. The contour plots cover an area of $13.3\lambda \times 13.3\lambda$. (b) Pair correlation functions for three to six interacting electrons with $\hbar\omega_0 = 4$ meV and $B = 20$ T (upper frames) and the corresponding classical configurations (lower frames). The black spots in each contour plot indicate r_0. The contour plots cover an area of $12\lambda \times 12\lambda$.

peaks together with the fixed electron form the corners of an equilateral triangle. Part (b) (upper frames) shows pair correlation functions, in the strong-field limit ($B = 20$ T), for various states of three to six spin-polarized interacting electrons. The form of the classical minimum-energy configuration is also shown (lower frames) for each electron number. Equilateral-triangular symmetry occurs for three electrons and more general forms of symmetry occur for larger electron numbers. The ground state of the four-electron system has square symmetry. In the case of five electrons the ground state has pentagonal symmetry ($J = 25$) but there are excited states which have square symmetry with one peak at the centre of the square ($J = 22$). For six electrons both sixfold ($J = 33$) and fivefold ($J = 35$) ground states are possible, while for seven electrons sixfold and sevenfold symmetry occurs (not shown; see [81, 83]). In each case the symmetry coincides with the symmetry of the classical minimum-energy configuration [85].

A radically different approach to the origin of the magic numbers is an interpretation in terms of composite fermions [87]. A composite fermion consists of an even number of magnetic flux quanta bound to an electron [88] and magic numbers are identified by considering how composite-fermion Landau levels are occupied. This leads to an approximate wave function that is used to approximate the total energy. The magic numbers correspond to compact occupation of the composite-fermion Landau levels. For $N \leqslant 5$ the composite-fermion approach gives the same magic numbers as the approaches based on symmetry. It also agrees well with the symmetry approach for six and seven electrons, although some discrepancies have been reported [81]; for example the composite-fermion approach does not predict the magic numbers $J = 40$ and $J = 50$ of the six-electron system. There are indications that the validity of the composite-fermion approach for bulk systems could be a consequence of the fact that a flux generates a 'correlation hole' which mimics the true one [88] and this may also

justify its validity for dots, but the issue has not yet been investigated.

The approaches based on exchange energy and symmetry are fairly consistent with each other and the link between them is the pair correlation function. The pair correlation functions for the special configurations that have adjacent occupations in angular momentum space can be shown [83] to have the same ring or centred-ring form as the exact pair correlation functions shown in figure 5. Thus it is entirely reasonable that these configurations should occur with high probability in the exact ground state and the angular momenta of these configurations are a good indicator of the ground-state correlations having the symmetry of the classical minimum. These issues have also been investigated in recent work by Ruan and Cheung [89]. The relation of the composite-fermion approach to the other approaches is less clear but the good agreement of all three approaches suggests that there is a link. It is likely that the composite-fermion construction results in a ground state with correlations that have the symmetry predicted by the other approaches but the mechanism that could lead to this is still an open question.

3.4. The limit of strong magnetic field

The pair correlation functions shown in part (a) of figure 5 acquire very sharp peaks as the magnetic field increases and extensive numerical studies have shown that this is generally true [83]. This suggests that the ground state in the strong-field limit is strongly localized about the classical potential minimum and the system may be pictured as an electron molecule [83,84]. A similar picture has been proposed for the state of a few electrons in a higher Landau level when the lower Landau levels are completely full [90]. The molecular picture provides an intuitive way of understanding the physics in the strong-field limit. Within this picture, approximate eigenstates found from a harmonic expansion of the Hamiltonian give the low-lying energy spectrum accurately and lead to all the known magic numbers. The remainder of this article is concerned with developing these ideas.

4. Two interacting electrons

The two-electron system is sometimes called quantum dot helium and is the simplest example of electron correlation in quantum dots. It has been studied extensively by exact-diagonalization [71], Hartree–Fock [64,65] and analytic approximation methods [91,92]. In addition, exact analytic treatments are available [93,94]. This section is concerned with one particular approximation which illustrates the molecular nature of the system in the large-angular-momentum limit.

4.1. Quantum ground states

The best way to study the two-electron system is to use CM and RM coordinates defined by $\boldsymbol{R} = (\boldsymbol{r}_1 + \boldsymbol{r}_2)/2$ and $\boldsymbol{r} = (\boldsymbol{r}_1 - \boldsymbol{r}_2)/2$ respectively, where $\boldsymbol{r}_1$ and $\boldsymbol{r}_2$ are the individual electron coordinates. Since $\boldsymbol{A}$ is linear in coordinates and $r_1^2 + r_2^2 = 2(R^2 + r^2)$, the Hamiltonian separates into

$$H = H_{CM} + H_{RM} \tag{6}$$

where

$$H_{CM} = \frac{1}{4m^*}\left(\boldsymbol{p}_{CM} + 2e\boldsymbol{A}(\boldsymbol{R})\right)^2 + m^*\omega_0^2 R^2 \tag{7}$$

$$H_{RM} = \frac{1}{4m^*}\left(\boldsymbol{p}_{RM} + 2e\boldsymbol{A}(\boldsymbol{r})\right)^2 + m^*\omega_0^2 r^2 + \frac{e^2}{8\pi\epsilon\epsilon_0 r} \tag{8}$$

and the momenta are $\boldsymbol{p}_{CM} = -\mathrm{i}\hbar\boldsymbol{\nabla}_R$ and $\boldsymbol{p}_{RM} = -\mathrm{i}\hbar\boldsymbol{\nabla}_r$. The eigenstates of the two-electron system are easy to study because of this separation into a sum of one-electron Hamiltonians. For larger numbers of electrons such a drastic simplification does not occur and the transformation to CM and RM coordinates is not even unique. One possible transformation, which is particularly suitable for dealing with molecular states, is described in section 5.

The eigenstates, ψ_{CM}, of H_{CM} are the Fock–Darwin states given by equation (2). The eigenstates, ψ_{RM}, of H_{RM} are eigenstates of the RM angular momentum and have the form $\psi_{RM} = \exp(-\mathrm{i}J_{RM}\chi)\phi(r)$ where J_{RM} is the RM angular momentum quantum number, χ is a polar angle and $\phi(r)$ is the radial function for the RM motion. This function and the energy of the RM motion, E_{RM}, are determined by the equation

$$\frac{-\hbar^2}{4m^*}\frac{1}{r}\frac{\mathrm{d}}{\mathrm{d}r}\left(r\frac{\mathrm{d}\phi}{\mathrm{d}r}\right) + \left[\frac{L^2}{4m^*r^2} + m^*\Omega^2r^2 + \frac{e^2}{8\pi\epsilon\epsilon_0 r} + \frac{\omega_c L}{2}\right]\phi(r) = E_{RM}\phi(r) \tag{9}$$

where, $L = -\hbar J_{RM}$. The spatial part of the full wave function is the product $\psi_{CM}\psi_{RM}$ and the total-angular-momentum quantum number is $J = J_{CM} + J_{RM}$ where J_{CM} is the quantum number for CM angular momentum

The molecular behaviour of the system in the high-angular-momentum limit becomes evident on simplifying equation (9). Putting $u(r) = \sqrt{r}\phi(r)$ (the factor $\sqrt{r}$ is suggested by the form of the area element in polar coordinates) leads to

$$\frac{-\hbar^2}{4m^*}\frac{\mathrm{d}^2u}{\mathrm{d}r^2} + \left[\frac{L^2 - \hbar^2/4}{4m^*r^2} + m^*\Omega^2r^2 + \frac{e^2}{8\pi\epsilon\epsilon_0 r} + \frac{\omega_c L}{2}\right]u(r) = E_{RM}u(r). \tag{10}$$

In the large-angular-momentum limit the centrifugal potential, $L^2/4m^*r^2$, rapidly becomes large as r becomes small and the quantum ground state is fairly well localized about the minimum of the total potential. Therefore a good approximation to the ground state can be obtained by Taylor expanding the potential about its minimum. The $-\hbar^2/(16m^*r^2)$ term can be neglected and the position, a, of the minimum is given by

$$\left(\frac{L}{2m^*a^2}\right)^2 + \frac{e^2}{8\pi\epsilon\epsilon_0}\frac{1}{2m^*a^3} - \Omega^2 = 0. \tag{11}$$

This equation is the same as the equation that determines the radius of the minimum-energy classical configuration in which the two electrons move in circular orbits while remaining diametrically opposite each other (see the appendix). If the quantum state is strongly localized about the classical configuration, the corresponding physical picture is that of a 'diatomic electron molecule' that vibrates and rotates inside the quantum dot.

The ground-state energy of the electron molecule is found by substituting the Taylor expanded potential into equation (10). Thus the vibrational states satisfy the harmonic oscillator equation:

$$\left[\frac{-\hbar^2}{4m^*}\frac{\mathrm{d}^2}{\mathrm{d}\xi^2} + E_0 + m^*\omega_1^2\xi^2\right]u(\xi) = E_{RM}u(\xi) \tag{12}$$

where $\xi = r - a$, E_0 is the classical orbit energy, $\omega_1^2 = \omega_r^2 + 3\Omega^2$ and $\omega_r = L/(2m^*a^2(L))$. The oscillator frequency, ω_1, is identical to the vibration frequency of the classical perturbed orbit (see the appendix). Strictly speaking, the equation has to be solved subject to the boundary condition that $\phi(r)$ remains finite as $r \to 0$. However, this boundary condition is satisfied to a good approximation by the usual harmonic oscillator states because large L corresponds to large a so the amplitude of an oscillator state centred on a is negligible at the origin. Thus the approximate ground-state energy is

$$E = E_{CM} + E_{RM} + g^*B\mu_B S_z = E_{CM} + E_0 + \left(n + \tfrac{1}{2}\right)\hbar\omega_1 + g^*B\mu_B S_z \tag{13}$$

where n is the number of oscillator quanta and the last term is the Zeeman energy. The approximate ground-state energy is just the sum of the classical energy, the quantum zero-point energy associated with the RM and CM motion and the Zeeman energy. The terms neglected in the Taylor expansion and the correction to the centrifugal potential are of order $1/\sqrt{|L|}$ or smaller. Thus the approximation should describe the physics reasonably well in the large-angular-momentum limit.

It is instructive to consider what happens when the magnetic field becomes large. In this case high-angular-momentum states occur as absolute ground states because the classical minimum energy depends on L. The L-value that minimizes the classical energy increases with B (see the appendix); consequently the J-value of the quantum ground state also increases with B. It is shown in the appendix (equation (A.5)) that the classical angular momentum, L^*, that minimizes E_0 is given by

$$L^{*3/2} = \frac{1}{16\pi\epsilon\epsilon_0}\frac{\sqrt{2m^*\Omega}}{(\Omega - \omega_c/2)}. \tag{14}$$

In quantum mechanics the J-value must be an integer and one of the two integers closest to $-L^*/\hbar$ is a good approximation to the ground-state J-value. The classical L^*-value increases monotonically with B and this results in a step-like increase of the quantum J-value. Thus the high-angular-momentum states occur as absolute ground states when the magnetic field is large. In the large-J_{RM} and large-B limit, $\omega_r \sim \Omega$, so $\sqrt{\omega_r^2 + 3\Omega^2} \sim 2\Omega \sim \omega_c$ and the oscillator length scale $\lambda^2 = \hbar/2m^*\Omega$ becomes small. This means that the potential in equation (10) acquires a deep minimum as B becomes large and the approximation leading to equation (12) becomes very good. Thus the electrons are strongly localized around the classical orbit and this is consistent with the general idea that the physics simplifies in the large-B limit when the cyclotron frequency is large and the cyclotron length is small. The physical picture of an electron molecule is very accurate in this limit.

The molecular picture gives some insight into the abrupt changes in dot radius shown in figure 3. The classical orbit radius is proportional to $\sqrt{L}$ (see the appendix) so it jumps when the angular momentum increases abruptly. When the quantum state is localized about the classical orbit the jump in the dot radius drives an increase in the effective dot size. This effect is certainly found in numerical studies of few-electron systems and may be related to the charge redistributions found experimentally by Oosterkamp *et al* [55]. Another interesting consequence of the molecular picture is that the angular momentum transitions become regularly spaced in the strong-field limit (see the appendix) for special combinations of confinement and interaction potentials, such as r^2 confinement and $1/r$ interaction. It may be possible to use this effect to probe the potential in a real dot [83].

The possible values of J are restricted to those compatible with the total spin because the two-electron state formed from the product of RM, CM and spin states has to be anti-symmetric. The CM ground state always has $J_{CM} = 0$ and is symmetric. The RM state is symmetric when J_{RM} is even and anti-symmetric when J_{RM} is odd. Thus spin-polarized ($S = 1$) ground states must have odd values of J and spin-unpolarized ($S = 0$) states must have even values. These are the magic numbers for the two-electron system. When the magnetic field is increased the J-value increases and, in addition, the system undergoes singlet–triplet transitions until the field is so strong that the Zeeman energy makes spin-polarized states energetically favourable.

4.2. Quantum excited states

The two-electron system has CM and RM excitations. The CM excitation energies are identical to the Fock–Darwin excitation energies and can be measured in far-infra-red (FIR) optical

absorption experiments. There are two types of low-lying RM excitation. One is accompanied by a change in RM angular momentum, $\Delta J_{RM} \neq 0$, and the other has $\Delta J_{RM} = 0$. Roughly speaking, the $\Delta J_{RM} \neq 0$ excitation is an angular excitation while the $\Delta J_{RM} = 0$ excitation is a radial excitation and the corresponding molecular picture is that of rotational and vibrational excitations respectively. The molecular vibration energy is $\hbar\omega_1$ while the rotational energy is found from the difference of the energies of a ground state and an absolute ground state. A peculiar feature of the rotational excitations of the two-electron system is that odd values of ΔJ_{RM} are impossible unless the spin state also changes. In contrast, when $N > 2$, excitations with arbitrary values of $\Delta J_{RM} \neq 0$ are possible without a change of spin.

4.3. Accuracy of the molecular picture

Figure 6 (top frame) shows ground-state energies for two spin-polarized electrons. The solid line shows the results of the molecular approximation and the diamonds give the results of the exact numerical diagonalization. The remaining lines show the classical energy and the sum of the classical energy and quantum zero-point energy—the zero-point energy is the dominant component in the very strong-field regime. It is clear that the exact and approximate

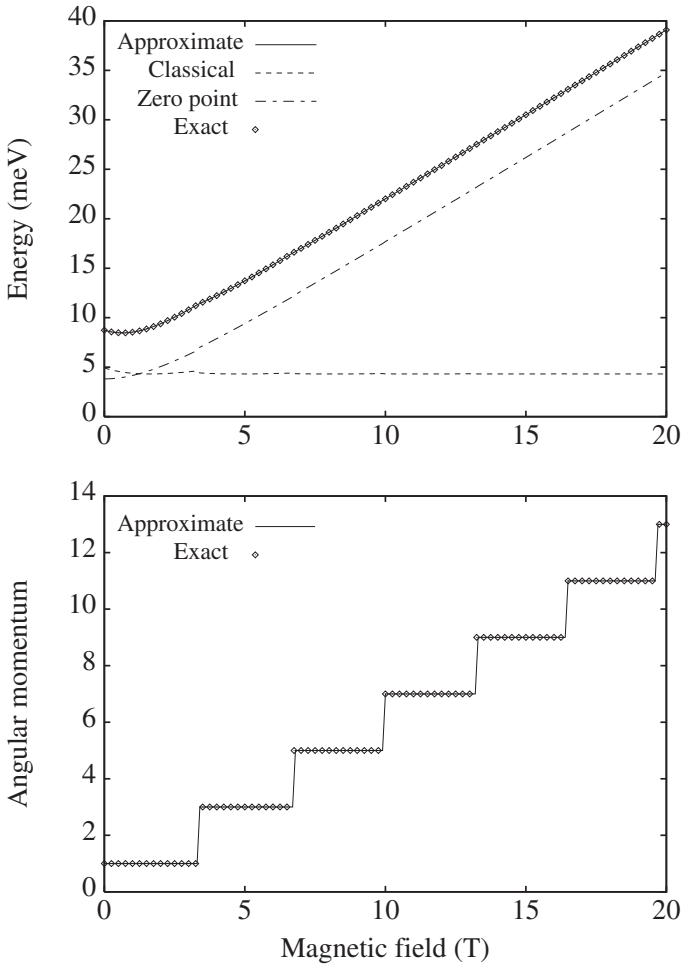

Figure 6. The magnetic field dependence of the exact ground-state energy and angular momentum of two spin-polarized interacting electrons with $\hbar\omega_0 = 2$ meV compared with approximate results based on the molecular picture.

energies agree surprisingly well even in the small-angular-momentum regime. They are within 0.002 meV for $J = 1$, $B = 0$ T and within 0.0002 meV for $J = 13$, $B = 20$ T. For comparison the numerical accuracy is about ± 0.002 meV for $J = 1$, $B = 0$ T and $\pm 0.000\,001$ meV for $J = 13$, $B = 20$ T. The bottom frame of figure 6 shows the exact ground-state J-value compared with the approximate value determined from equation (14). Again, it is clear that the molecular and exact results agree well. The transition fields are well reproduced and the spacing of the transition fields is nearly regular, in agreement with the general discussion after equation (14)—the equation gives a transition field spacing of 3.32 T while the numerically calculated spacing is 3.2 ± 0.1 T. The lowest RM excitation energy, ΔE, with $\Delta J_{RM} = 0$ is shown in figure 7. The top frame shows the excitation energy as a function of J_{RM} at $B = 20$ T and it can be seen that the numerical and molecular results agree well in the large-J_{RM} limit. They are within 0.01 meV for $J_{RM} = 9$ and 0.002 meV for $J_{RM} = 19$. The bottom frame shows the excitation energy for $J = 19$ relative to the non-interacting excitation energy, i.e. $\Delta E - 2\hbar\Omega$, as a function of magnetic field. The two energies are within about 0.002 meV throughout the field range.

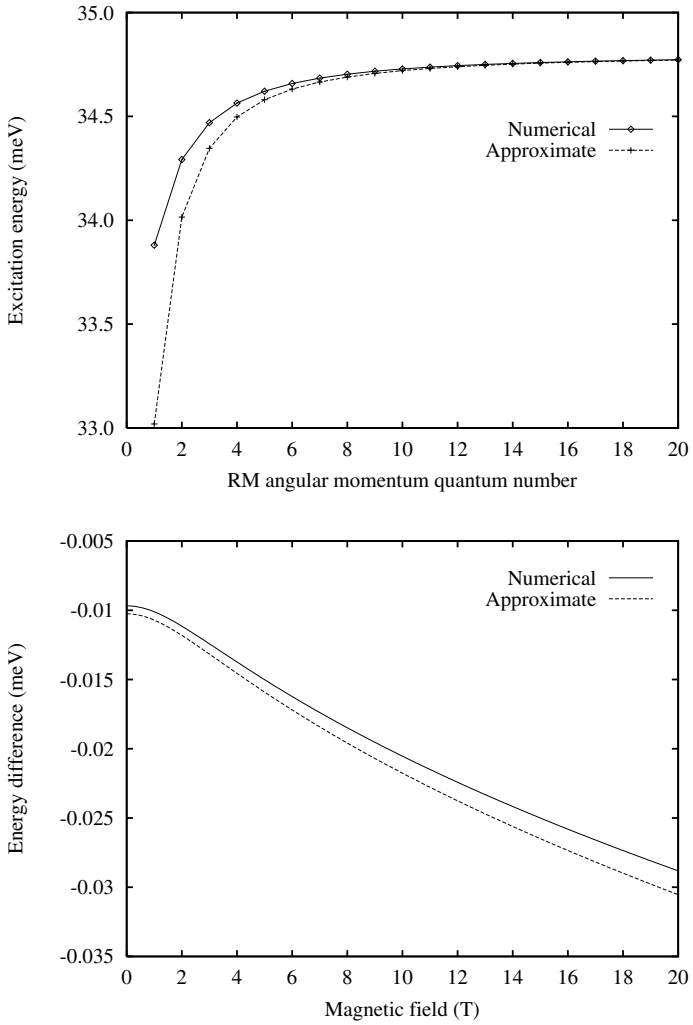

Figure 7. The exact RM excitation energy of two spin-polarized interacting electrons with $\hbar\omega_0 = 2$ meV compared with approximate results based on the molecular picture. Upper frame: ΔE as a function of J_{RM}; lower frame: $\Delta E - 2\hbar\Omega$ as a function of B at $J_{RM} = 19$.

One reason for the astonishing accuracy of the molecular picture is that the cubic term in the Taylor expansion of the potential is of odd parity. Thus it does not affect the energy to first order in perturbation theory and the lowest-order corrections to the energy are of order $1/|L|$, rather than $1/\sqrt{|L|}$. These corrections come from the second-order perturbation due to the cubic term in the Taylor expansion and the first-order perturbation due to the quartic term. To evaluate the energy to order $1/|L|$ it is also necessary to include the $-\hbar^2/(16m^*r^2)$ correction to the centrifugal potential because this is of order $1/a^2$ and hence of order $1/|L|$. After some tedious algebra it can be shown that, for $J_{RM} \neq 0$, the corrected excitation energy is $\Delta E + \delta E$, where

$$\delta E = \frac{3\hbar\omega_r}{4J'}\left[\frac{3\omega_r^2+2\Omega^2}{\omega_r^2+3\Omega^2}\left(\left(n+\frac{1}{2}\right)^2+\frac{1}{4}\right)-5\left(\frac{\omega_r^2+\Omega^2}{\omega_r^2+3\Omega^2}\right)^2\left(\left(n+\frac{1}{2}\right)^2+\frac{7}{60}\right)\right] \tag{15}$$

and $J' = \sqrt{J_{RM}^2 - 1/4}$. Clearly, the correction to ΔE is the difference of two terms which are of similar magnitude. In the large-J_{RM} and large-B limit the two terms partly cancel and δE approaches $\hbar\omega_c/8|J_{RM}|$. The accuracy of the molecular picture is probably related to this cancellation but the effect of higher-order corrections remains to be investigated.

5. Theory of electron molecular states

The analysis of the two-electron system has led to the physical picture of the electron molecule and shown that an approximation based on a harmonic expansion of the potential about the classical orbit radius works extremely well in the large-J_{RM} and large-B limit. This section is concerned with generalizing the picture to more electrons. It turns out that an equally accurate picture can be developed for up to at least six electrons but this requires some new concepts which are not needed to deal with the two-electron system. For instance, a special moving reference frame is needed in the N-electron case and the vibrational motion is affected by Coriolis forces. In addition, larger systems tend to have multiple potential minima and this affects the physics. Further, electron states must be anti-symmetric to satisfy the Pauli principle but an arbitrary product of CM, RM angular momentum, vibrational and spin states is not necessarily anti-symmetric and a group theoretical procedure is needed to identify the combinations of states that can be anti-symmetrized. An interesting feature of larger systems is that the combination of the spatial symmetry of the 'electron molecule' and the anti-symmetry required by the Pauli principle leads directly to magic number states and generally enriches the physics.

5.1. The Eckart frame

'Molecular states' are expected to be strongly localized about the classical minimum-energy orbit and are expected to have some symmetry. For example, the two-electron system has two electrons orbiting diametrically opposite each other and thus has twofold symmetry when viewed in a rotating frame. Similarly, in the three-electron minimum-energy orbit the electrons are at the corners of a rotating equilateral triangle. This raises the question of a suitable reference frame for the general N-electron case. Coriolis forces normally appear whenever motion is treated in a moving frame, although the two-electron system is an exceptional case where they do not affect vibrational motion. The presence of Coriolis forces leads to a Hamiltonian in which coordinates and momenta are coupled. It is desirable to use a frame in which this coupling is minimized and a suitable choice is the Eckart frame which has long been used to study the vibrational states of ordinary molecules [83, 95]. Recently, a geometrical

interpretation of the Eckart frame has been given which is based on the use of a gauge potential to describe the internal degrees of freedom of a molecule [96].

The Eckart frame is designed to make the angular momentum associated with vibrations about the classical minimum vanish to first order in displacements from the classical equilibrium positions, $\boldsymbol{a}_i$, that minimize the classical energy. This leads to the Eckart condition:

$$\sum_i \boldsymbol{a}_i \times \boldsymbol{r}_i' = \boldsymbol{0} \tag{16}$$

where the $\boldsymbol{r}_i'$ are positions relative to the CM and all vectors are in the Eckart frame. The special feature of the Eckart frame is that the coordinate–momentum coupling terms in the RM Hamiltonian are of second order in the displacements.

The classical RM Hamiltonian can be expressed in any coordinates, but in molecular physics, normal coordinates, Q_i, are often employed, so that the displacement from the equilibrium position is $\boldsymbol{\rho}_i = \sum_j \boldsymbol{Q}_{ij} Q_j$ where the $\boldsymbol{Q}_{ij}$ are elements of the matrix that relates Cartesian and normal coordinates. It is convenient to use the same coordinates to study electron states and the classical Eckart frame RM Hamiltonian can be expressed *exactly* in terms of them:

$$H_{RM} = \frac{1}{2}\mu(L_{RM} - L_v)^2 + \frac{1}{2m^*}\sum_{k=1}^{2N-3} P_k^2 + V + \frac{\omega_c}{2}L_{RM} \tag{17}$$

where L_{RM} is the RM angular momentum,

$$L_v = \sum_k \mathcal{Z}_k P_k \qquad \mathcal{Z}_k = \sum_{ij} (\boldsymbol{Q}_{ij} \times \boldsymbol{Q}_{ik}) \cdot \hat{\boldsymbol{k}} Q_j$$

and

$$\mu = I_0 \Big/ \left(I_0 + m^* \sum_{ij} \boldsymbol{a}_i \cdot \boldsymbol{Q}_{ij} Q_j \right)^2 .$$

Here P_j is the momentum conjugate to Q_j, I_0 is the equilibrium moment of inertia and V is the total potential (including confinement and interaction terms together with a term quadratic in the magnetic vector potential). The quantity L_v is an angular momentum associated with vibrational motion and it involves products of coordinates and momenta. The RM Hamiltonian is independent of the normal coordinates for CM and rotational excitations and involves only $2N - 3$ coordinates. One more coordinate is needed to describe the relative motion fully and this is an Euler angle, χ, that gives the orientation of the Eckart frame.

The quantum mechanical Eckart frame Hamiltonian is derived from the classical one by applying the Podolsky procedure (as described by Kemble [97], for example). The transformation to normal coordinates introduces a Jacobian into the normalization integral but it is more convenient [97] to have a wave function that *both* obeys an eigenvalue equation of the form $H_{RM}\Psi = E\Psi$ *and* is normalized with respect to the volume element $\mathrm{d}\chi\ \mathrm{d}Q_1 \cdots \mathrm{d}Q_{2N-3}$. Some lengthy manipulations are needed to eliminate the Jacobian and a consequence of them is that the quantum mechanical Eckart frame RM Hamiltonian has an additional potential term, $-\hbar^2\mu/8$, which is called the Watson term. The elimination of the Jacobian is analogous to the substitution $u = \sqrt{r}\phi$ used to derive equation (10), the transformed radial equation in the two-electron case, and the Watson term is analogous to the centrifugal potential correction in this equation. In fact, the only non-trivial normal mode in the two-electron case is radial and the two-electron Eckart frame Hamiltonian is identical to the two-electron RM Hamiltonian in equation (10). In general, the Watson term is of order $1/|L_{RM}|$, so can be neglected to lowest order. The Podolsky procedure then gives a quantum mechanical Eckart frame Hamiltonian that is the same as the classical one, equation (17), except that momenta are replaced by operators.

5.2. Equilibrium positions

The equilibrium positions can be found by setting the linear momenta, P_j, in equation (17) to zero and minimizing the resulting effective potential. The condition that the minimum occurs when all the displacements are zero leads to the equations

$$\frac{m^* L_{RM}^2}{I_0^2}\boldsymbol{a}_i - \boldsymbol{\nabla}_i V\big|_{\boldsymbol{r}_i'=\boldsymbol{a}_i} = \mathbf{0}. \tag{18}$$

These equations are similar to the equations that define Lagrangian orbits in celestial mechanics [99]. They can be solved to find the equilibrium positions of arbitrary numbers of electrons but the equilibrium positions for small numbers of electrons can be found in a simpler way. By symmetry, the net force on each electron is in the radial direction when the electrons are symmetrically distributed around a ring. Thus each electron moves in a circular orbit and the equilibrium configuration is a rotating symmetric polygon, for example a triangle for three electrons or a square for four electrons etc (see figure 5). As the electron number increases it becomes energetically favourable for one or more electrons to be inside the polygonal ring. This first happens for six electrons and the resulting configuration consists of a pentagon with an electron at the centre. When the electron number is increased further very complicated configurations occur in which the electrons are arranged in concentric shells. These configurations have been studied as a function of electron number by various numerical methods [85, 100–102] and some general analytic results are also available [83, 103]. As the electron number becomes large, the energy of the system has multiple minima which are very close in energy and special techniques are needed to locate the global minimum [101, 102].

5.3. Vibrational motion

The classical Hamiltonian, H', for the vibrational motion about the steady-state rotation is found by Taylor expanding the Eckart frame RM Hamiltonian, which is *exact*, about one of the equilibrium configurations. Retaining terms up to second order in momenta and coordinates leads to the following Hamiltonian energy relative to the classical minimum energy:

$$H' = \frac{1}{2m^*}\sum_{j=1}^{2N-3} P_j^2 + \sum_{j=1}^{2N-3}\sum_{k=1}^{2N-3} C_{jk} Q_j P_k + \frac{m^*}{2}\sum_{j=1}^{2N-3}\omega_{nj}^2 Q_j^2 \tag{19}$$

where

$$C_{jk} \equiv (-L_{RM}/I_0)\sum_i \boldsymbol{Q}_{ij} \times \boldsymbol{Q}_{ik} \cdot \hat{\boldsymbol{k}}$$

is a Coriolis coupling coefficient and ω_{nj} is the frequency of the jth normal mode. In the strong-field limit, $L_{RM}/I_0 \sim \omega_c/2$, so the Coriolis coupling coefficients are large and it is essential to retain the coordinate–momentum coupling terms to obtain accurate results. The higher-order terms in the Taylor expansion are of order $1/\sqrt{L_{RM}}$ or smaller, so the molecular picture is particularly accurate when the angular momentum is large.

The frequencies of the vibrational motion are found by assuming harmonic time dependence of the normal-mode amplitudes, Q_j, and conjugate momenta, P_j. This leads to an eigenvalue equation that gives the classical vibrational modes and frequencies [98, 99]. The quantum vibrational states are found by replacing the coordinates and momenta in equation (19) with operators obeying canonical commutation relations. A canonical transformation of the resulting quantum Hamiltonian leads to a Hamiltonian of the form $\sum_j \hbar\omega_j(a_j^\dagger a_j + 1/2)$, where the ω_j are the vibrational frequencies and the $a_j^\dagger$ and a_j, respectively, are raising and lowering operators [83]. Thus the quantum vibrational states are expressed in terms of the

raising operators acting on the vibrational ground state. This is true for all electron numbers and enables the quantum vibrational states to be written down when the classical vibrational modes and frequencies are known. In general, these modes have to be found numerically but an analytic solution is available for the three-electron case [83, 84].

5.4. Permutational symmetry

Anti-symmetric electron states are constructed by applying the anti-symmetrization operator to rotational–vibrational states. There are $N!$ equilibrium configurations, each corresponding to a different permutation of the electrons. Some of these configurations are connected by rotations but others are not. For example, equilateral-triangular configurations of three electrons with vertices labelled in cyclic order, like ${}_1{}^2{}_3$ and ${}_3{}^1{}_2$, can be rotated into each other but it is not possible to rotate ${}_1{}^2{}_3$ into ${}_2{}^1{}_3$. The configurations that cannot be rotated into each other are called symmetrically equivalent. A harmonic expansion can be done about each of the symmetrically equivalent configurations and the resulting quantum states are degenerate. In reality tunnelling among symmetrically equivalent states breaks the degeneracy but this effect is small in the large-angular-momentum limit when the states are strongly localized. In this case good approximate electron states can be constructed by anti-symmetrizing a rotational–vibrational state localized about any one of the symmetrically equivalent minima.

In the harmonic approximation, and before anti-symmetrization, the rotational–vibrational states have the general form

$$\Psi = \psi_{CM} \exp(-\mathrm{i}J_{RM}\chi) f_{J_{RM},n_1,\ldots,n_{2N-3}}(Q_1, \ldots, Q_{2N-3})\psi_{spin}(S_z). \tag{20}$$

The factors are states associated with various degrees of freedom: ψ_{CM} is the CM wave function; $\exp(-\mathrm{i}J_{RM}\chi)$ is the wave function for rotation about the CM; f is a vibrational wave function with $n_1, \ldots, n_{2N-3}$ the numbers of quanta in each vibrational mode; ψ_{spin} is the spin function and S_z is the z-component of the total spin, S. In general, the anti-symmetrized states can be written in the form $\hat{A}\Psi$, where $\hat{A}$ is the anti-symmetrization operator. However, not every rotational–vibrational state can be used to construct an anti-symmetric state because there are some quantum number combinations for which $\hat{A}\Psi$ is *exactly zero*. To find the quantum states of the N-electron molecule it is necessary to determine the quantum number combinations for which $\hat{A}\Psi$ is not zero. The total energy of these states is the sum of the classical equilibrium energy and the energies corresponding to the various factors in equation (20). The resulting equation for the total energy is the many-electron analogue of equation (13), that is

$$E = E_{CM} + E_0 + \sum_{i=1}^{2N-3} \left(n_i + \frac{1}{2}\right)\hbar\omega_i + g^*\mu_B B S_z. \tag{21}$$

Thus the total energy can be found very simply once the allowed combinations of quantum numbers have been identified.

The physics of the electron molecular ground-state energy is determined by whether a ground vibrational state can be used to construct an anti-symmetric state. If the anti-symmetrized ground rotational–vibrational state is non-zero, the electron molecular state will have the lowest energy possible and will approximate one of the magic number ground states. Otherwise the electron molecular state must have some additional energy because an excited vibrational state has to be used to form the lowest-energy anti-symmetric state. It turns out that ground vibrational states only lead to anti-symmetric states when J_{RM} takes one of the magic values. This remarkable finding is consistent with the observation made earlier that the magic numbers reflect the symmetry of the classical equilibrium configurations.

The reason why particular angular momenta are associated with the point symmetry of particular 'electron molecules' is that there are some special permutations that are equivalent

to rotations. The question of whether anti-symmetrization of Ψ gives a zero or non-zero result can be decided by considering the sub-group of these special permutations, although all $N!$ permutations are needed to construct the anti-symmetric state. In general, a permutation of the laboratory frame electron coordinates has a very complicated effect on the Eckart frame coordinates, χ and Q_i. However, the effect of the special permutations is just to rotate the Euler angle χ and to rotate and permute the Eckart frame displacements. The rotation of χ changes Ψ by a phase factor and an anti-symmetric state can only be constructed if the product of this phase and compensating phases from the vibrational and spin factors is ± 1, depending on whether the permutation is odd or even. The phase factors are determined by the point symmetry of the equilibrium configuration; hence the magic angular momenta are a direct consequence of symmetry.

In general, some group theory is needed to determine the phase factors, but the physics can be illustrated with the special case of the three-electron, spin-polarized ground state which can be treated without resort to the general procedure. In this case, the classical minimum-energy configuration is equilateral triangular and the special permutations are equivalent to threefold rotations, for example (123). The vibrational ground state is symmetric under these rotations while the CM ground state and spin state are symmetric under all permutations. The symmetry properties are therefore determined solely by the angular momentum factor $\exp(-\mathrm{i}J_{RM}\chi)$. The permutations that are equivalent to threefold rotations have even parity, so the angular momentum factor must be invariant under them if the electron ground state is to be anti-symmetric. This restricts J_{RM} to multiples of 3 and, because $J_{CM} = 0$ in the ground state, the total J must also be a multiple of 3 as found in the numerical calculations leading to figure 3.

To anti-symmetrize the rotational–vibrational states it is convenient to choose spin functions that change phase under the cyclic permutations that are equivalent to rotations. For example, when $N = 3$ and $S_z = 1/2$ and the classical minimum has threefold symmetry, a suitable spin function is

$$|{}_{\uparrow}{}^{\uparrow}{}_{\downarrow}\rangle + \varepsilon|{}_{\downarrow}{}^{\uparrow}{}_{\uparrow}\rangle + \varepsilon^2|{}_{\uparrow}{}^{\downarrow}{}_{\uparrow}\rangle$$

where $\varepsilon = \exp(2\pi \mathrm{i}k_s/3)$, k_s can take the values 0, 1, 2 and the positions of the arrows indicate that the spin function is associated with triangular symmetry. Analogous spin functions can be constructed for larger numbers of electrons. For m-fold symmetry the phase factor is $\varepsilon = \exp(2\pi \mathrm{i}k_s/m)$ and k_s is an integer in the range $0 \leqslant k_s \leqslant m-1$. It can be shown [83] that the vibrational states also change phase under cyclic permutations. The phase change for the ith vibrational state can be characterized by an integer $k_v(i)$ that is analogous to k_s and lies in the range $0 \leqslant k_v(i) \leqslant m-1$. Group theoretical analysis [10, 83, 84] then leads to the result than an anti-symmetric state can only be constructed when J_{RM}, k_s and the numbers of quanta n_i in each vibrational mode satisfy

$$J_{RM} + k_s + \sum_{i=1}^{2N-3} n_i k_v(i) \equiv \begin{cases} 0 \bmod m & m \text{ odd} \\ m/2 \bmod m & m \text{ even} \end{cases} \tag{22}$$

and this equation gives all the magic numbers that are found in numerical calculations for electron numbers up to 7.

6. Physics of few-electron molecules

The pair correlation functions discussed in section 3.4 and the analysis of the two-electron system given in section 4 indicate that the electron molecular picture is accurate in the limit of strong magnetic field. This is confirmed in the present section by comparing approximate

and exact results for ground-state and excitation energies of a few electrons in a GaAs dot with $\hbar\omega_0 = 4$ meV in a 20 T magnetic field. The physics develops subtly with electron number as the effective potential energy of the system acquires multiple minima. It is particularly interesting to see how different aspects of the physics emerge as electrons are added to the system one by one.

6.1. Ground states

The three-electron system is the smallest for which the Eckart frame approach is needed [10, 83, 84]. Ground-state energies calculated from equation (21) are shown in figure 8 for $S = 3/2$ (upper frame) and $S = 1/2$ (lower frame). Small oscillations in the ground-state

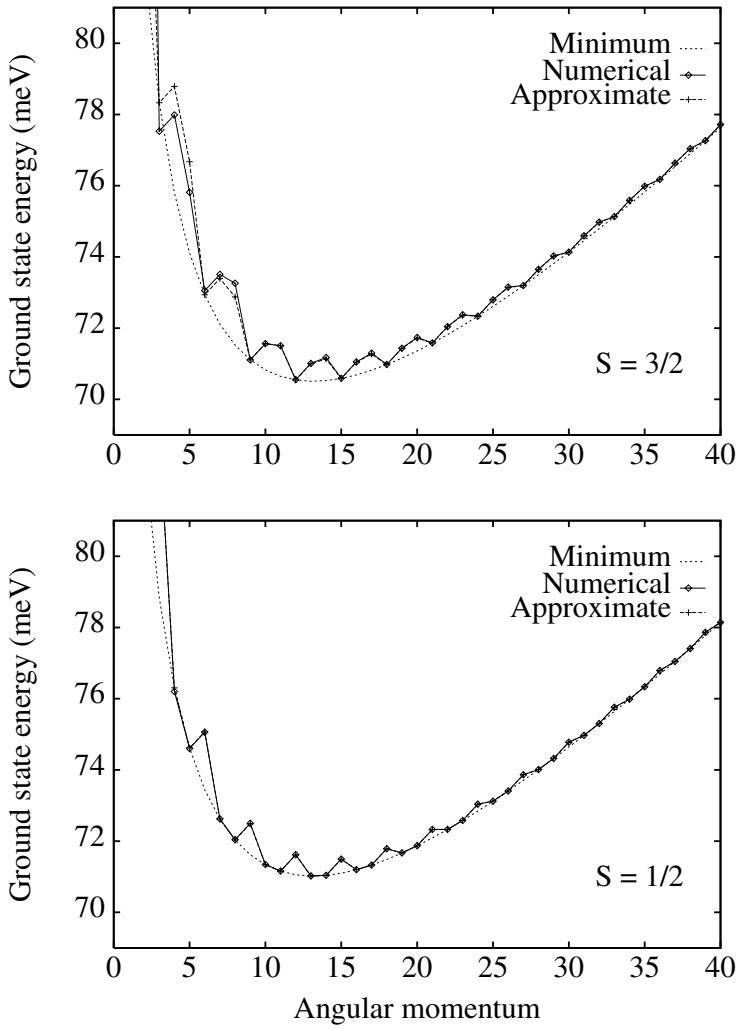

Figure 8. Exact ground-state energies of three interacting electrons for $\hbar\omega_0 = 4$ meV compared with energies based on the molecular picture. The diamonds and plus signs give the energies and the lines are to guide the eye. The dashed line, labelled minimum, is the sum of the classical energy and the quantum zero-point energy of the molecular system.

energy, which occur because anti-symmetric states cannot be constructed from molecular ground states, are clearly visible in both the molecular and exact results for both values of the total spin. The molecular and exact results are almost indistinguishable throughout the J-range when $S = 1/2$ and for J greater than about 10 when $S = 3/2$. For $J \geqslant 30$ the results typically agree to about three parts per million [83].

The molecular picture also describes the four-electron ground states very well. Ground-state energies for all three possible values of the total spin are shown in figure 9. Small oscillations in energy are again evident and the molecular and exact results are indistinguishable on the scale of the figure when $J \geqslant 22$. When J becomes very large the molecular results become very accurate; for example, the agreement for the $S = 0$ ground-state energy at $J = 34$ (not shown in the figure) is about 0.003%. The four-electron system is the smallest for which there is numerical evidence for tunnelling between symmetrically equivalent minima [83]. One prediction of the anti-symmetrization procedure for constructing molecular states is that there are degenerate levels with different values of S, for example, the ground states with $S = 0$ and $S = 2$ when $J \equiv 2 \bmod 4$ and $S = 0$ and $S = 1$ when $J \equiv 0 \bmod 4$. Numerical results show that these levels are split but the splitting decreases as J increases and eventually becomes smaller than the Zeeman spin splitting. Thus the high field suppresses tunnelling between symmetrically equivalent minima.

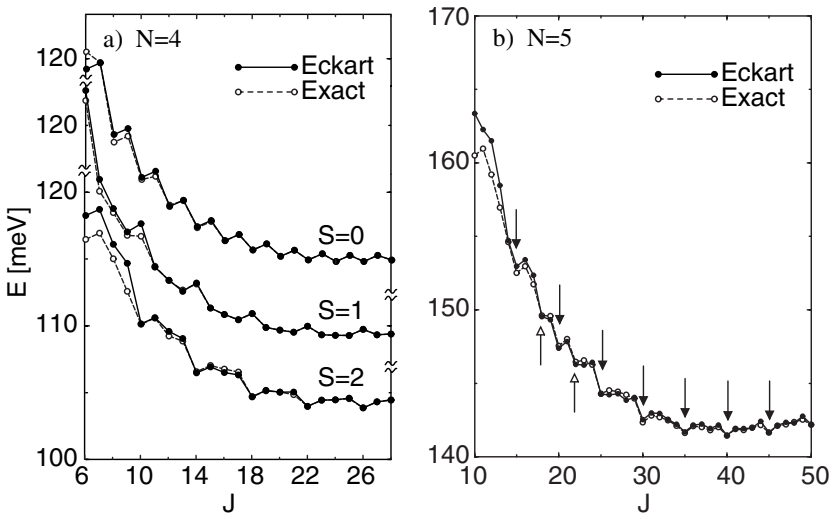

Figure 9. Exact ground-state energies of four ($S = 0$) and five ($S = 5/2$) interacting electrons for $\hbar\omega_0 = 4$ meV compared with energies based on the molecular picture. The circles give the energies and the lines are to guide the eye.

The spin-resolved pair correlation function [104,105] of the four-electron system at $S = 0$ has a very interesting structure (figure 10). The magic numbers in this case are multiples of 2 but the spin correlation pattern alternates between two types depending on whether $J \equiv 0 \bmod 4$ or $J \equiv 2 \bmod 4$. For $J \equiv 2 \bmod 4$, nearest-neighbour sites tend to have opposite spins but they tend to have like spins when $J \equiv 0 \bmod 4$ and this is a consequence of the anti-symmetrization condition, equation (22). Anti-symmetry requires that $k_s = 0$ when $J_{RM} \equiv 2 \bmod 4$ and $k_s = 2$ when $J_{RM} \equiv 0 \bmod 4$. The way this affects the spin correlation can be understood by rewriting the spin states in terms of RVB (resonating valence bond) states [106]. These states were originally conceived for lattice systems, and are $S = 0$ basis functions constructed by covering the lattice with spin-singlet pairs like $(1/\sqrt{2})(|\uparrow\downarrow\rangle - |\downarrow\uparrow\rangle)$. Explicit forms of

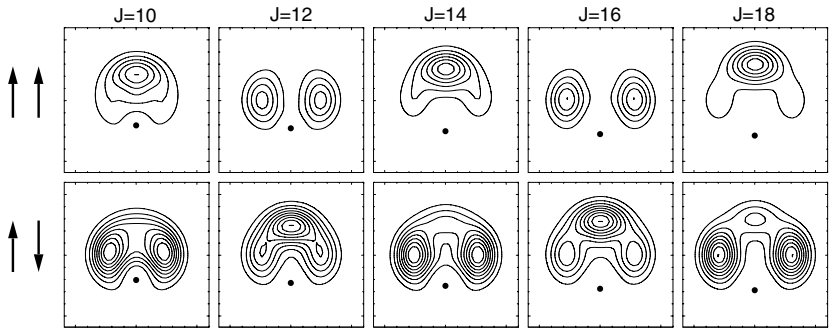

Figure 10. Spin-resolved ground-state pair correlation functions for four interacting electrons with $S = 0$ and $\hbar\omega_0 = 4$ meV. The contour plots cover an area of $12\lambda \times 12\lambda$.

these states for small numbers of electrons can be found in the literature [107] and appropriate products of them are known to span the $S = 0$ subspace [108, 109]. In the four-electron case the spin functions characterized by k_s are, except for a normalization factor:

$$k_s = 0: \qquad \left|\begin{matrix}\uparrow\uparrow\\ \downarrow\downarrow\end{matrix}\right\rangle + \left|\begin{matrix}\downarrow\downarrow\\ \uparrow\uparrow\end{matrix}\right\rangle + \left|\begin{matrix}\uparrow\downarrow\\ \uparrow\downarrow\end{matrix}\right\rangle + \left|\begin{matrix}\downarrow\uparrow\\ \downarrow\uparrow\end{matrix}\right\rangle - 2\left[\left|\begin{matrix}\downarrow\uparrow\\ \uparrow\downarrow\end{matrix}\right\rangle + \left|\begin{matrix}\uparrow\downarrow\\ \downarrow\uparrow\end{matrix}\right\rangle\right] \tag{23}$$

$$k_s = 2: \qquad \left|\begin{matrix}\uparrow\uparrow\\ \downarrow\downarrow\end{matrix}\right\rangle + \left|\begin{matrix}\downarrow\downarrow\\ \uparrow\uparrow\end{matrix}\right\rangle - \left|\begin{matrix}\uparrow\downarrow\\ \uparrow\downarrow\end{matrix}\right\rangle - \left|\begin{matrix}\downarrow\uparrow\\ \downarrow\uparrow\end{matrix}\right\rangle \tag{24}$$

and in the singlet pair covering representation they become

$$k_s = 0: \qquad \square\square - \square\square \tag{25}$$

$$k_s = 2: \qquad \square\square + \square\square \equiv \boxtimes \tag{26}$$

where $\square \equiv (1/\sqrt{2})(|\uparrow\downarrow\rangle - |\downarrow\uparrow\rangle)$ represents a spin-singlet pair [104, 105]. The tendency for opposite spins to occur at opposite corners of the square for $J \equiv 0 \bmod 4$ is consistent with equation (26). For larger numbers of electrons it is possible to express the spin states in terms of RVB states but the interpretation of the spin-resolved pair correlation function is complicated by the near-degeneracies which occur when tunnelling between symmetrically equivalent configurations is small.

The five-electron system is the smallest for which the effect of competing potential minima is apparent [104]. In this case there are two different classical equilibrium configurations. The global minimum configuration is pentagonal but there is a local minimum configuration which consists of a square with one electron in the centre. Both configurations must be taken into account to calculate the energy as a function of J in the molecular picture. The ground-state energy, found by taking the lowest of these two energies, is shown in figure 9. The main sequence of minima at $J \equiv 0 \bmod 5$ corresponds to the pentagonal configuration (filled arrows) but it is accompanied by subsidiary minima at $J \equiv 2 \bmod 4$ which correspond to the square configuration (open arrows). The absolute ground state always corresponds to the pentagonal configuration and at $J = 40$ the agreement with the exact-diagonalization results is better than 0.2%.

The six-electron system is probably the most interesting of all because there are some subtle effects which determine its ground state. Contrary to intuition, the classical hexagonal ring is unstable with respect to a distortion in which alternating electrons move inwards and

outwards (figure 11, lower frames). Thus there are two degenerate threefold minimum-energy configurations instead of one sixfold configuration. There is also a pentagonal minimum-energy configuration and this is the global minimum configuration. However, the energy difference between the two configurations is relatively small—about 0.57 meV when $\hbar\omega_0 = 4$ meV and the magnetic field is 20 T. The energy of the distorted hexagonal configuration as a function of the distortion is shown in figure 11 (upper left frame). The energy of the threefold minima is just 1 μeV less than that of the hexagonal ring and special care is needed to find them numerically [104]. At first sight, the existence of the threefold minima seems inconsistent with the magic numbers of the six-electron system, some of which correspond to sixfold symmetry [81,83]. One particularly interesting feature of the six-electron system is the way in which the sixfold symmetry emerges when the system is treated quantum mechanically.

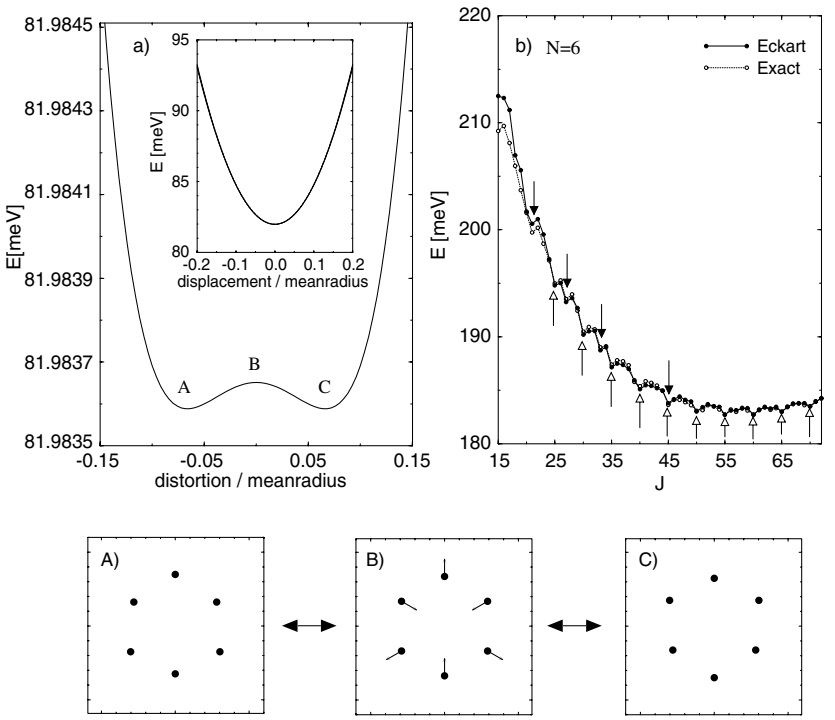

Figure 11. Potential energy as a function of distortion (top left frame), the form of distortion (bottom frames), and ground-state energies of six interacting electrons for $\hbar\omega_0 = 4$ meV and $S = 3$. The circles give the energies and the lines are to guide the eye. The inset to the top left frame gives the potential energy for a vibrational mode whose displacement pattern is the same as the distortion pattern.

To understand how the sixfold symmetry is recovered, consider the ground state of the double minimum associated with the distortion. This state can be approximated variationally as a superposition of states localized on the two degenerate threefold minima. Suppose a wave function, ϕ, that is localized about one of these minima has been found. Then a wave function localized about the second minimum has the form $R_6\phi$, where R_6 is the operator for a $2\pi/6$ rotation. (The states $R_6^3\phi$ and $R_6^5\phi$ are also localized about the second minimum but are not independent of $R_6\phi$.) A variational approximation to the ground state of the distorted system is the symmetric state $\psi = \phi + R_6\phi$. The rotational–vibrational state is therefore

$\exp(-\mathrm{i}J\chi)(\phi + R_6\phi)$ and under a $2\pi/6$ rotation this transforms like

$$R_6 \exp(-\mathrm{i}J\chi)(\phi + R_6\phi) = \exp(-2\pi\mathrm{i}/6)\exp(-\mathrm{i}J\chi)(R_6\phi + R_6^2\phi)$$
$$= \exp(-2\pi\mathrm{i}/6)\exp(-\mathrm{i}J\chi)(\phi + R_6\phi)$$

where the last step follows from the fact that the ground state in the threefold minimum is invariant under threefold rotations. Thus ψ transforms under rotations like a sixfold state.

The variational approach gives one way of calculating approximate energies of the six-electron system but it is rather tedious. In practice, it has been found that an even simpler approximation gives good agreement with numerical data. This is based on the observation that the distortion of the hexagonal ring is only about 20% of the wave-function length scale, λ. Thus the energy can be approximated by replacing the wave function for the distorted system by one localized about the hexagonal ring. The hexagonal ring has one unstable vibrational mode. The displacement pattern of the corresponding normal mode is the same as the distortion pattern shown in figure 11. The potential energy as a function of this displacement from the hexagonal position is shown in the inset to the top left frame of figure 11. This energy is not exactly parabolic but is well approximated by a fitted parabola—the fitted parabola is also shown in the inset and is almost indistinguishable from the true potential energy. All the vibrational modes become stable if the true potential is replaced by the fitted parabola and the Eckart frame theory can then be used to obtain approximate eigenstates which have the required sixfold symmetry. This enables approximate energies to be found from the formalism in section 5.3 but is only valid when the distortion is small. The variational approach or even an exact solution of the Schrödinger equation for the distortional degree of freedom would be required when the distortion is not small.

Ground-state energies for six spin-polarized electrons calculated in the molecular picture are shown in figure 11 (top right frame) together with results from exact numerical diagonalization. The minima in the main series have angular momentum $J \equiv 0 \bmod 5$ (open arrows) and correspond to the pentagonal configuration. In addition, there is a series of minima at $J \equiv 3 \bmod 6$ which correspond to hexagonal symmetry (filled arrows). When the angular momentum is large, $J \geqslant 60$, the molecular picture gives results accurate to better than 0.4%.

The final, and most interesting, feature of the six-electron system is that it is the smallest system for which tunnelling between symmetrically inequivalent minima is important. Pentagonal and hexagonal symmetry are allowed to coexist when the angular momentum satisfies both $J \equiv 0 \bmod 5$ and $J \equiv 3 \bmod 6$. Because the corresponding equilibrium configurations have similar energies, tunnelling between them is important and the pair correlation functions for these states are radically different from those for the molecular states [81, 83]. This is illustrated in figure 12. The lower left frame ($J = 50$) is the pair correlation function for the absolute ground state at $B = 17.5$ T. All the pair correlation functions are for ground states at $B = 17.5$ T and the indicated values of J. The pair correlation function at $J = 51$ clearly corresponds to sixfold symmetry and the one at $J = 40$ to fivefold symmetry. The pair correlation function for $J = 45$, when both fivefold and sixfold symmetry are allowed, exhibits some loss of symmetry. The peaks on the outer ring are less sharp than at $J = 40$ and $J = 50$ and the peak at the centre is less distinct. Clearly, the $J = 45$ state cannot be described as molecular and perhaps a suitable description is 'liquid-like'. The 'liquid-like' states are allowed to occur only when the angular momentum is in the sequence $15, 45, 75, \ldots$. When these J-values are converted to effective Landau level filling factors [63] with the aid of the formula $\nu = N(N-1)/2J$, it is found that the 'liquid-like' states occur when $\nu = 1, 1/3, 1/5, \ldots$. That is, at the same odd-denominator fractions where fractional quantum Hall liquids occur in bulk systems.

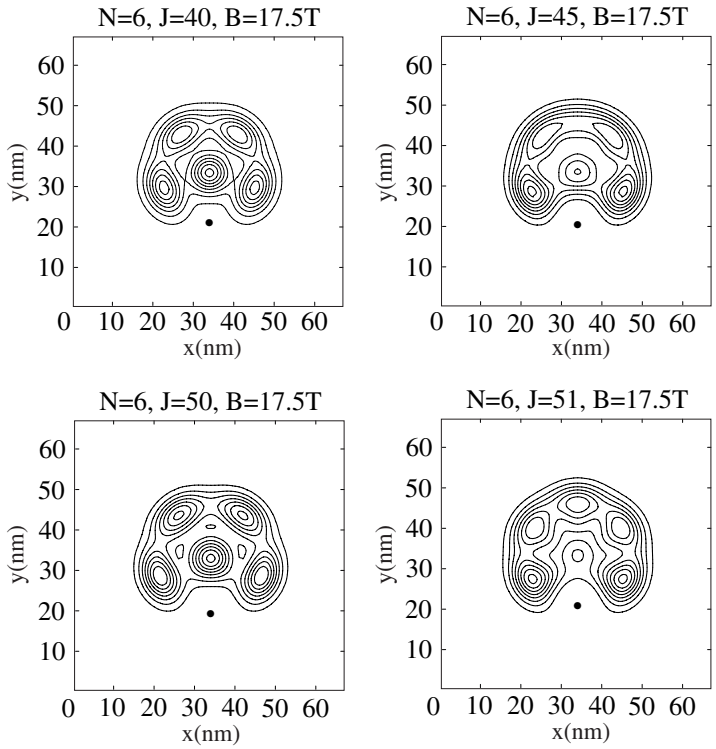

Figure 12. Six-electron pair correlation functions for molecular ($J = 40, 50, 51$) and liquid-like ($J = 45$) states. The contour plots cover an area of $22\lambda \times 22\lambda$.

6.2. Excited states

An N-electron parabolic dot has the same types of low-lying excitation (section 4.2) as a two-electron parabolic dot: CM excitations, RM excitations with $\Delta J_{RM} \neq 0$ and RM excitations with $\Delta J_{RM} = 0$. The RM excitations are affected by electron correlation and those with $\Delta J_{RM} \neq 0$ are accurately reproduced in the electron molecular picture. This can be seen in figures 8 to 11. There are higher-energy states with angular momenta different from that of the absolute ground state. These excited states are CM or RM excitations relative to the absolute ground state, or in some cases with $|\Delta J_{RM}| > 1$ combinations of both CM and RM excitations. The electron molecular picture reproduces all these excitation energies to about the same accuracy as the absolute-ground-state energy.

The RM excitation energies for $\Delta J_{RM} = 0$ can be found in the molecular picture by using the method described in section 5 to find the smallest vibrational excitation that is compatible with anti-symmetry. Three-electron RM excitation energies obtained in this way are shown in figure 13 for both $S = 1/2$ and $S = 3/2$ ground states [83]. The exact-diagonalization results are absent at $J_{RM} = 10$ and $J_{RM} \leqslant 8$ because intra-Landau level excitations do not exist in these cases. The exact results are broadly in agreement with the molecular ones. When $S = 1/2$ the molecular picture is very good. In particular, the oscillations in the excitation energy, which are a consequence of the anti-symmetrization condition (equation (22)), are well reproduced. The agreement at $J_{RM} = 40$ is about 3%. When $S = 3/2$ the molecular picture is accurate to about 8% in the large-angular-momentum limit but at low angular momenta

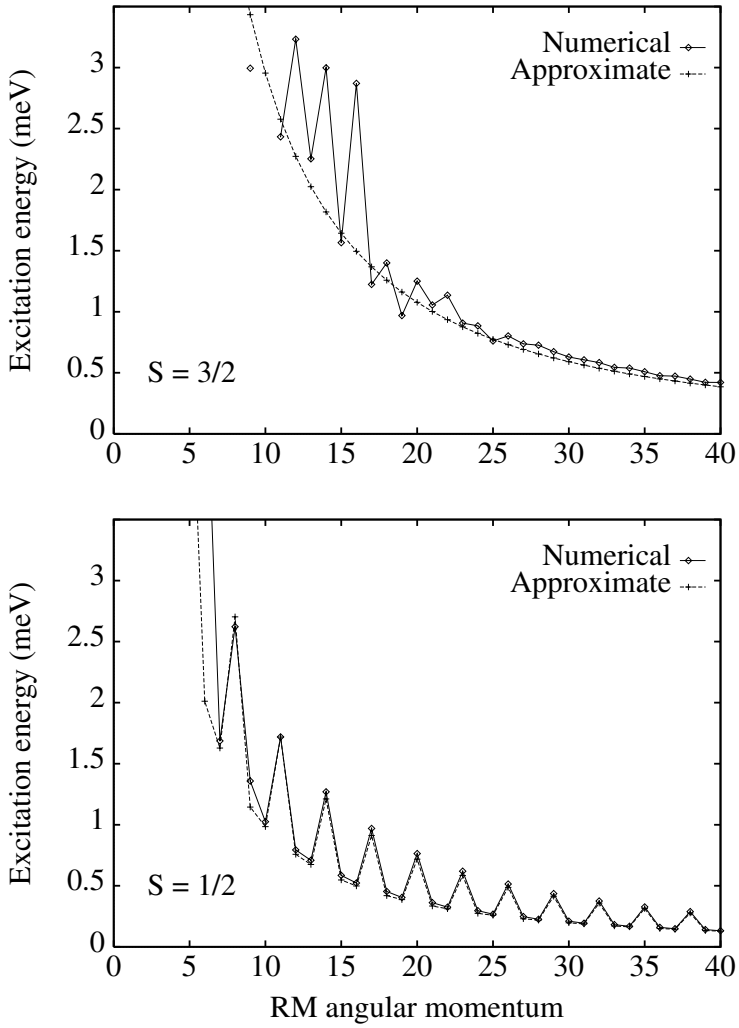

Figure 13. Exact RM excitation energies for three interacting electrons with $\hbar\omega_0 = 4$ meV compared with results based on the molecular picture. The diamonds and plus signs give the energies and the lines are to guide the eye.

the numerical excitation energy fluctuates, although the general trend is in agreement with the molecular results. Four-electron RM excitation energies are shown in figure 14. The anti-symmetrization condition again leads to excitation patterns characteristic of the total spin and these patterns occur in the numerical data. For instance, when $S = 2$ large excitation energies are predicted to occur at $J_{RM} \equiv 1 \bmod 4$ and $J_{RM} \equiv 2 \bmod 4$ and small ones at $J_{RM} \equiv 3 \bmod 4$ and $J_{RM} \equiv 0 \bmod 4$. This pattern can be seen in the numerical data when $J_{RM} \geqslant 41$. Similarly, the excitation energy is predicted to oscillate with period 4 for $S = 1$ and change smoothly with J_{RM} when $S = 0$ and these trends occur in the numerical data when J_{RM} is sufficiently high. The quantitative accuracy of the molecular picture at $J_{RM} = 50$ is about 3–8%. As in the three-electron system, the molecular excitation pattern tends to occur in the numerical data at the lowest J_{RM}-values when the system is not spin polarized: for $S = 1$ the pattern occurs above $J_{RM} = 20$, but for $S = 2$ it occurs above $J_{RM} = 40$ while for $S = 0$

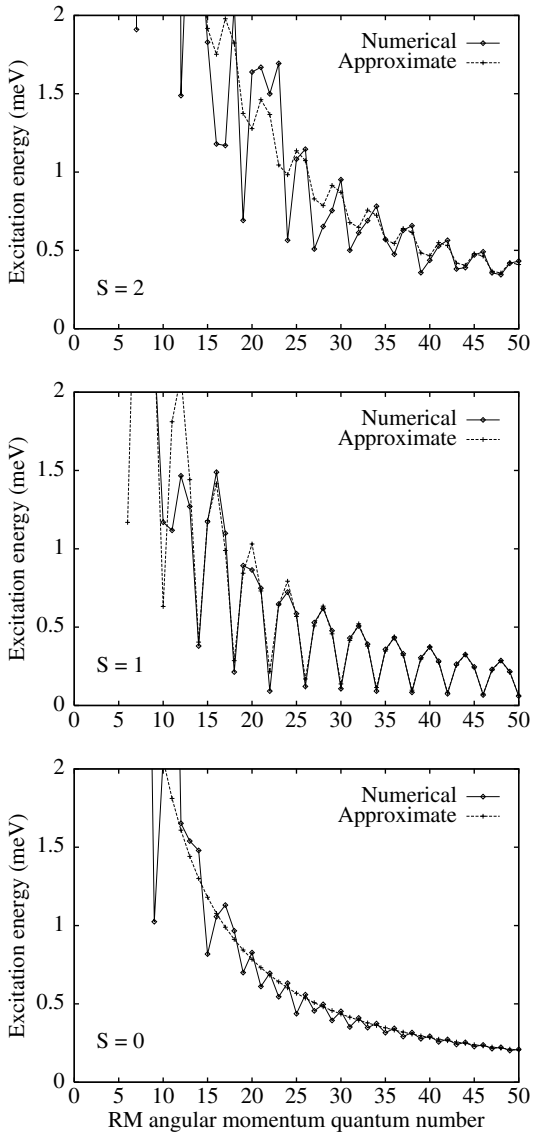

Figure 14. Exact RM excitation energies for four interacting electrons with $\hbar\omega_0 = 4$ meV compared with results based on the molecular picture. The diamonds and plus signs give the energies and the lines are to guide the eye.

it occurs above about $J_{RM} = 35$, although the numerical data have some oscillations which persist up to $J_{RM} = 50$.

Physically, the origin of the spin-dependent excitation patterns is related to the way the rotational, vibrational and spin states change phase under the permutations that are equivalent to rotations. The phase changes are characterized by the quantum numbers J_{RM}, k_v and k_s respectively and the quantum number combinations for both the ground and excited states must satisfy equation (22). Typically there are a few different spin states and a few different vibrational states. For example, there are two different low-energy vibrational states when

$N = 4$ and three different spin states when $N = 4$, $S = 1$ and $S_z = 1$. Usually, several different combinations of the quantum numbers satisfy equation (22) and the excitation energy patterns are found by looking for the quantum number combinations that correspond to the smallest excitation energy [83].

The tendency for the molecular excitation pattern to emerge at particularly large J_{RM}-values when the system is spin polarized is a consequence of the fact that there is just one spin state (with $k_s = 0$) in this case. Consequently it is not possible to compensate for the vibrational phase by adjusting k_s and this means that the excited states have to be constructed from larger numbers of vibrational quanta. For example, at least two quanta are required when $N = 4$ and $S = 2$. Physically, these highly excited states have a greater spatial extent than the lower states and should be more sensitive to processes neglected in the simple molecular picture, such as tunnelling between symmetrically equivalent minima and anharmonicity. Hence it is quite reasonable that the molecular description of the RM excitations at low J_{RM}-values is best when the system is not spin polarized.

7. Discussion

The molecular picture provides an extremely good and accurate description of ground states and low-lying excited states of few-electron quantum dots. The picture is intuitively appealing and gives quantitative information at relatively low cost. However, the picture is not yet complete. One of the outstanding issues is the extent to which it can describe larger systems. Another is experimental verification.

It would be good to have a better understanding of systems with more than six electrons. The accuracy of the molecular picture seems to be fairly independent of electron number for up to six electrons. There is apparently a small loss of accuracy in going from two to six electrons but the numerical results for various electron numbers have not been obtained at the same Landau level filling factors: exact-diagonalization results for the larger electron numbers cannot be obtained for large enough J to reach the same small filling factor, $\nu = N(N-1)/2J$, as for the smaller electron numbers. The agreement of the exact-diagonalization and molecular data for the larger electron numbers would probably improve if the exact diagonalization could be done for large enough angular momentum. As the number of electrons increases it is likely that effects of distortion and multiple minima, similar to those that occur in the six-electron case, will become more important. If multiple energy minima occur, the nature of the ground state might be determined by selection rules, similar to the rule that determines when the fivefold and sixfold states of the six-electron system are allowed to mix. In a larger system there could be more than two minima and this raises the interesting possibility of states where no mixing, complete mixing or mixing of a subset of symmetry types occurs. Physically, no mixing and complete mixing would correspond to molecular and liquid-like states, respectively, but mixing of a subset of symmetry types would correspond to a new type of state whose physical nature is not yet clear. As the number of electrons becomes very large, quantum Hall liquids should be found amongst the low-J ground states while the high-J ground states are more likely to correspond to Wigner crystals. The quantum Hall liquids only occur at odd-denominator filling factors. It has been suggested that this could be related to symmetry effects similar to those that determine whether the six-electron ground state is liquid-like [83]—physically the ground state would be a liquid if it was able to explore all the potential minima. There has been some investigation of the consequences of symmetry effects for larger systems, and they do seem to account for the observed filling factors [110, 111], but the theory involves a number of approximations and the problem is still open to some extent.

It would also be interesting to know whether the molecular picture can account for the

excitations of larger systems. It would probably give a good description of the rotational excitations of molecular states but its accuracy for vibrational excitations probably depends on how many vibrational quanta are needed to construct the anti-symmetric excited states and on the spin polarization. For large systems having n-fold symmetry with large n, large numbers of quanta would be needed to construct spin-polarized excited states and the accuracy of the molecular picture could be reduced unless the angular momentum was very large.

Experimental verification of the molecular picture is a challenging task. It is difficult to probe the pair correlation function that would give direct information about the physical state of electrons in a quantum dot. Instead, the nature of the state has to be inferred from transport and optical data which are sensitive to energy levels. The task is made more difficult by the decoupling of RM and CM motion in a parabolic dot which makes it hard to probe the RM motion which is affected by electron correlation. Thermodynamic properties are not affected by this problem and are known to be sensitive to interactions [36, 70, 71] but are difficult to measure experimentally. An alternative is to introduce some RM and CM coupling in a controlled way to infer the nature of the ground state. Raman scattering [42] is one possibility. Another is to work with laterally coupled [112] or vertically coupled dots [113–116, 119]. A particularly interesting feature of vertically coupled dots is that molecular correlation can occur either within each dot or across the two dots. The latter leads to three-dimensional electron molecules which have been investigated with quantum [116–119] and classical [120, 121] mechanics. If the confinement energy, $\hbar\omega_0$ in each of the two dots is different, the RM and CM motions couple and FIR spectra are sensitive to interactions [116, 119, 122] and could give information about the state of the dot. The effect could be enhanced by deliberately increasing the confinement energy difference. Another way of manipulating a dot to probe its state might be to apply a lateral shearing electric field with some external electrodes. Increasing the electric field would crack the electron molecule and abrupt changes in its form would lead to abrupt changes in the addition energy which could be observed in transport experiments. Classical Monte Carlo calculations indicate that molecular and liquid states could be distinguished in this way and there would be a unique signature for each electron number [123]. Finally and very speculatively, it might be possible to couple electrons in a pillar dot to the vibrational modes of the pillar.

Probably the most challenging experimental task of all would be to detect the oscillatory form of the vibrational excitations as a function of RM angular momentum. This would require fairly low-energy excitations to be probed and, in addition, a way of preparing the system in a non-magic ground state. This seems very difficult but if it could be achieved it would give direct evidence for a molecular states because the predicted excitation patterns are a direct consequence of the electron molecular picture.

Acknowledgments

This work was supported by the UK Engineering and Physical Sciences Research Council, the European Union, Leicester University and partly by a Grant-in-Aid 'Spin controlled Semiconductor Nanostructures' from the Japanese Ministry of Education. PAM is grateful for the hospitality of the Department of Physics, University of Tokyo, where this work was completed.

Appendix. Classical treatment of two interacting electrons

This appendix is concerned with the interesting and important low-energy circular orbits of two interacting point charges, which can be found by elementary methods [59]. It is possible

to find general expressions for all the RM orbits but these expressions involve elliptic integrals and are somewhat uninformative [124].

In the minimum-energy configuration of the two-electron system, the centre of mass is at rest in the centre of the dot and the electrons move in circular orbits while remaining diametrically opposite to each other. The effective Hamiltonian, H_{co}, that determines the orbit radius is found from H_{RM} (equation (8)) and is given by

$$H_{co} = \frac{L^2}{4m^*a^2} + \frac{e^2}{8\pi\epsilon\epsilon_0 a} + m^*a^2\Omega^2 + \frac{\omega_c}{2}L \tag{A.1}$$

where a is the orbit radius and $L = \sum_i (\boldsymbol{r}_i \times \boldsymbol{p}_i)\cdot\hat{\boldsymbol{k}}$ is the total angular momentum. The orbit radius as a function of L and B can found by minimizing H_{co}, or directly from Newton's laws. For each magnetic field, there is a family of circular orbits, whose radii are related to L via

$$\left(\frac{L}{2m^*a^2}\right)^2 + \frac{e^2}{8\pi\epsilon\epsilon_0}\frac{1}{2m^*a^3} - \Omega^2 = 0. \tag{A.2}$$

One of these orbits minimizes the total energy and this orbit can be found by solving equation (11) to find $a(L)$ and then minimizing the total energy with respect to L.

The exact value of a can be found numerically but to understand the physics it is better to look at the large-L limit. In this case a is approximately given by

$$a = \sqrt{\frac{|L|}{2m^*\Omega}} + \mathrm{O}\left(\frac{1}{|L|}\right). \tag{A.3}$$

Thus a increases with $|L|$ at fixed B. In addition, it decreases with B at fixed L because Ω increases with B. The total energy in the same approximation is

$$E_0 \simeq \left(|L|\Omega + L\frac{\omega_c}{2}\right) + \frac{e^2}{8\pi\epsilon\epsilon_0}\sqrt{\frac{2m^*\Omega}{|L|}} + \mathrm{O}\left(\frac{1}{|L|^2}\right). \tag{A.4}$$

The first term is similar to the energy of a Fock–Darwin state, while the second is a Coulomb correction. The total energy as a function of L always has a minimum. To examine this, it is convenient to use $\hbar$ as the unit of angular momentum. The substitution $L = -\hbar J$ defines a classical J-value which is a real number. The classical J-value, J^*, that minimizes E_0 is

$$J^{*3/2} = \frac{1}{16\pi\epsilon\epsilon_0}\frac{\sqrt{2m^*\Omega}}{\hbar^{3/2}(\Omega - \omega_c/2)} \tag{A.5}$$

and this is a monotonically increasing function of B. In the high-field limit this becomes

$$B = \frac{m^*}{e}\left[\frac{e^2}{16\pi\epsilon\epsilon_0}\frac{\sqrt{m^*}}{\hbar^{3/2}\omega_0^2}\right]^{-2/3} J^* \tag{A.6}$$

so J^* is linear in B. The physics of the classical ground state is now clear: the angular momentum of the minimum-energy orbit increases with field and, in the high-field limit, both the optimal L and Ω increase linearly with B, so the optimal orbit radius approaches a constant.

The increase of the classical J^*-value is similar to the increase of the quantum ground-state J-value but in the quantum case the J-values are restricted to integers. If this constraint is applied to the classical system, the optimal J-value is either $[J^*]$ or $[J^*]+1$ where $[J^*]$ is the integer part of J^*, depending on which of these integers gives the lowest value of E_0. With this restriction, the classical system exhibits a series of transitions in which the J-value increases in a step-like way when B is increased. In addition, a oscillates with B because a increases abruptly whenever J increases, then decreases with a further increase of B.

The classical treatment also gives some insight into the physics of the transitions and the way they depend on confinement and interaction potentials. In the classical picture a transition occurs when two orbits with different angular momenta have the same energy, that is when $E_0(J, B) = E_0(J+1, B)$, or approximately when $\partial E_0/\partial J = 0$. This is just the condition that defines J^*, so the transition fields in the high-field limit can be found from equation (A.6). This shows that the transition field is proportional to J and therefore the transitions are regularly spaced in the high-field limit. This behaviour is quite peculiar. It only occurs for special types of potential and the combination of r^2 confinement and $1/r$ interaction is one of them. It is easy to repeat the classical treatment for a general confinement potential of the form r^q and an interaction of the form r^{-p}. In this case the approximate transition fields in the high-field regime are given by

$$B = \frac{m^*}{e}\left[\frac{e^2}{16\pi\epsilon\epsilon_0}\frac{\sqrt{m^*}}{\hbar^{3/2}\omega_0^2}\right]^{-2/3}(J^*)^{(p+q)/3}. \tag{A.7}$$

and it is clear that the linear J-dependence only occurs when $p + q = 3$.

There are perturbed classical trajectories whose energy is slightly higher than that of the circular orbits, and physically, these trajectories correspond to vibrations about the steady-state circular motion. The two-electron system in two dimensions has four degrees of freedom and four excitation modes. Formally, these modes can be found by applying Routh's procedure to analyse the perturbed motion about the steady-state orbit [98, 125], but it is easier to find them by using physical arguments. Because the Hamiltonian separates, two of the modes are associated with CM with and two with RM motion. One of the RM modes is rotational and the remaining one is vibrational. These two modes are orthogonal and the rotational motion involves purely angular displacements. Therefore the vibrational mode must be radial with the displacements of the two electrons of equal magnitude and in opposite directions. The effective Hamiltonian for the radial motion is therefore

$$H' = \frac{p_\xi^2}{4m^*} + \frac{L^2}{4m^*(a+\xi)^2} + \frac{e^2}{8\pi\epsilon\epsilon_0(a+\xi)} + m^*(a+\xi)^2\Omega^2 + \frac{\omega_c}{2}L \tag{A.8}$$

where ξ is the electron displacement and $p_\xi = m^*\dot{\xi}$. Taylor expanding this to second order about $\xi = 0$ leads to the equation of motion

$$\ddot{\xi} + (\omega_r^2 + 3\Omega^2)\xi = 0 \tag{A.9}$$

where $\omega_r = L/(2m^*a^2(L))$. Thus the radial mode is stable and its frequency is $\sqrt{\omega_r^2 + 3\Omega^2}$. This coincides with the frequency that appears in the Schrödinger equation for the vibrational states (equation (12)).

References

[1] Jacak L, Hawrylak P and Wójs A 1998 *Quantum Dots* (Berlin: Springer)
[2] Chakraborty T 1999 *Quantum Dots* (Amsterdam: Elsevier)
[3] Arakawa Y and Yariv Y 1986 *IEEE J. Quantum Electron.* **22** 1887
[4] Schmitt-Rink S, Miller D A B and Chemla D S 1987 *Phys. Rev.* B **35** 8113
[5] Kirstaedter N, Ledentsov N N, Grundmann M, Bimberg D, Ustinov N V, Ruvimov S S, Maximov M V, Kopev P S, Alferov Z I, Richter U, Werner P, Gosele U and Heydenreich J 1994 *Electron. Lett.* **30** 1416
[6] Imamura K, Sugiyama Y, Nakata Y, Muto S and Yokoyama N 1995 *Japan. J. Appl. Phys.* **34** L1445
[7] Bryant G W 1987 *Phys. Rev. Lett.* **59** 1140
[8] Häusler W, Kramer B and Măsek J 1991 *Z. Phys.* B **85** 435
[9] Laughlin R B 1983 *Phys. Rev.* B **27** 3383
[10] Maksym P A 1993 *Physica* B **184** 385

[11] Häusler W and Kramer B 1993 *Phys. Rev.* B **47** 16 353
[12] Jauregui K, Häusler W and Kramer B 1993 *Europhys. Lett.* **24** 581
[13] Jefferson J H and Häusler W 1996 *Phys. Rev.* B **54** 4936
[14] Creffield C E, Häusler W, Jefferson J H and Sarkar S 1999 *Phys. Rev.* B **59** 10 719
[15] Egger R, Häusler W, Mak C H and Grabert H 1999 *Phys. Rev. Lett.* **82** 3320
Egger R, Häusler W, Mak C H and Grabert H 1999 *Phys. Rev. Lett.* **83** 462
[16] Fertig H A 1997 *Perspectives in Quantum Hall Effects* ed S Das Sarma and A Pinczuk (New York: Wiley)
Lea M J and March N H 1989 *Int. J. Quantum Chem.* S **23** 717
[17] Demel T, Heitmann D, Grambow P and Ploog K 1990 *Phys. Rev. Lett.* **64** 788
[18] Sikorski C and Merkt U 1989 *Phys. Rev. Lett.* **62** 2164
[19] Tarucha S, Austing D G, Honda T, Vanderhage R J and Kouwenhoven L P 1996 *Phys. Rev. Lett.* **77** 3613
[20] Weis J, Haug R J, von Klitzing K and Ploog K 1993 *Phys. Rev. Lett.* **71** 4022
[21] Tulkki J and Heinämäki A 1995 *Phys. Rev.* B **52** 8239
[22] Solimany L and Kramer B 1995 *Solid State Commun.* **96** 471
[23] Peeters F M, Matulis A and Ibrahim I S 1996 *Physica* B **227** 131
[24] Mallon G P and Maksym P A 1998 *Physica* B **256** 186
[25] Marzin J M, Gérard J M, Izraël A, Barrier D and Bastard G 1994 *Phys. Rev. Lett.* **73** 716
[26] Tarucha S, Austing D G, Honda T, van der Hage R J and Kouwenhoven L P 1997 *Japan. J. Appl. Phys.* **36** 3917
[27] Madhav A V and Chakraborty T 1994 *Phys. Rev.* B **49** 8163
[28] Ezaki T, Mori N and Hamaguchi C 1997 *Phys. Rev.* B **56** 6428
[29] Maksym P A 1998 *Physica* B **251** 233
[30] Lier K and Gerhardts R R 1993 *Phys. Rev.* B **48** 14 416
[31] Maksym P A and Bruce N A 1997 *Physica* E **1** 211
[32] Bruce N A and Maksym P A 2000 *Phys. Rev.* B **61** 4718
[33] Meurer B, Heitmann D and Ploog K 1992 *Phys. Rev. Lett.* **68** 1371
[34] Heitmann D and Kotthaus J P 1993 *Phys. Today* **46** (6) 56
[35] Brey L, Johnson N F and Halperin B I 1989 *Phys. Rev.* B **40** 10 647
[36] Maksym P A and Chakraborty T 1990 *Phys. Rev. Lett.* **65** 108
[37] Pfannkuche D and Gerhardts R R 1991 *Phys. Rev.* B **44** 13 132
[38] Gudmundsson V, Brataas A, Grambow P, Meurer B, Knurth T and Heitmann D 1995 *Phys. Rev.* B **51** 17 744
[39] Maksym P A, Hallam L D and Weis J 1995 *Physica* B **212** 213
[40] Hallam L D, Weis J and Maksym P A 1996 *Phys. Rev.* B **53** 1452
[41] Zrenner A 1996 *Surf. Sci.* **361/2** 756
[42] Steinebach C, Krane R, Biese G, Schüller C, Heitmann D and Eberl K 1996 *Phys. Rev.* B **54** 14 281
[43] Kastner M A 1993 *Phys. Today* **46** (1) 17
[44] McEuen P L, Foxman E B, Meirav U, Kastner M A, Meir Y, Wingreen N S and Wind S J 1991 *Phys. Rev. Lett.* **66** 1926
[45] Su Bo and Goldman V J 1992 *Phys. Rev.* B **46** 7644
[46] Tewordt M, Martín-Moreno L, Law V J, Kelly M J, Newbury R, Pepper M, Ritchie D A, Frost J E F and Jones G A C 1992 *Phys. Rev.* B **46** 3948
[47] Johnson A T, Kouwenhoven L P, de Jong W, van der Vaart N C, Harmans C J P M and Foxon C T 1992 *Phys. Rev. Lett.* **69** 1592
[48] Heinzel T, Wharam D A, Kotthaus J P, Böhm G, Klein W, Tränkle G and Weimann G 1994 *Phys. Rev.* B **50** 15 113
[49] van der Vaart N C, Ruyter van Stevenick M P, Harmans C J P M and Foxon C T 1994 *Physica* B **194** 1251
[50] Kouwenhoven L P, Oosterkamp T H, Danoesastro M W S, Eto M, Austing D G, Honda T and Tarucha S 1997 *Science* **278** 1788
[51] Ashoori R C, Störmer H L, Weiner J S, Pfeiffer L N, Pearton S J, Baldwin K W and West K W 1992 *Phys. Rev. Lett.* **68** 3088
[52] Ashoori R C, Störmer H L, Weiner J S, Pfeiffer L N, Baldwin K W and West K W 1993 *Phys. Rev. Lett.* **71** 613
[53] Kouwenhoven L, Jauhar S, Orenstein J, McEuen P L, Nagamune Y, Motohisa I and Sakaki H 1994 *Phys. Rev. Lett.* **73** 3443
[54] Blick R H, Haug R J, von Klitzing K and Eberl K 1996 *Surf. Sci.* **361/2** 595
[55] Oosterkamp T H, Jansen J W, Kouwenhoven L P, Austing D G, Honda T and Tarucha S 1999 *Phys. Rev. Lett.* **82** 2931
[56] Chakraborty T 1992 *Comment. Condens. Matter Phys.* **16** 35
[57] Johnson N F 1995 *J. Phys.: Condens. Matter* **7** 965
[58] Ashoori R C 1996 *Nature* **379** 413

[59] Maksym P A 1997 *From Quantum Mechanics to Technology (Springer Lecture Notes in Physics vol 477)* ed Z Petru, J Przystawa and K Rapcewicz (Berlin: Springer)
[60] Sohn L L, Kouwenhoven L P and Schön G (ed) 1997 *Mesoscopic Electron Transport (NATO ASI Series E: Applied Sciences, vol 345)* (Dordrecht: Kluwer)
[61] Fock V 1928 *Z. Phys.* **47** 446
[62] Darwin C G 1930 *Proc. Camb. Phil. Soc.* **27** 86
[63] Girvin S M and Jacah T 1984 *Phys. Rev.* B **28** 4506
[64] Pfannkuche D, Gudmundsson V and Maksym P A 1993 *Phys. Rev.* B **47** 2244
[65] Pfannkuche D, Gerhardts R R, Maksym P A and Gudmundsson V 1993 *Physica* B **189** 6
[66] Palacios J J, Martín-Moreno L, Chiappe G, Louis E and Tejedor C 1994 *Phys. Rev.* B **50** 5760
[67] Macucci M, Hess K and Iafrate G J 1993 *Phys. Rev.* B **48** 17 354
[68] Ferconi M and Vignale G 1994 *Phys. Rev.* B **50** 14 722
[69] Chamon C de C and Wen X G 1994 *Phys. Rev.* B **49** 8227
[70] Maksym P A and Chakraborty T 1992 *Phys. Rev.* B **45** 1947
[71] Wagner M, Merkt U and Chaplik A V 1992 *Phys. Rev.* B **45** 1951
[72] Johnson N F and Payne M C 1993 *Phys. Rev. Lett.* **70** 1513
[73] Pfannkuche D and Ulloa S 1995 *Phys. Rev. Lett.* **74** 1194
[74] Hawrylak P and Pfannkuche D 1993 *Phys. Rev. Lett.* **70** 485
[75] Hawrylak P 1994 *Solid State Commun.* **93** 915
[76] Pietiläinen P, Halonen V and Chakraborty T 1995 *Physica* B **212** 256
[77] Halonen V, Pietiläinen P and Chakraborty T 1996 *Europhys. Lett.* **33** 377
[78] Hawrylak P 1993 *Phys. Rev. Lett.* **71** 3347
[79] Yang S R, MacDonald A H and Johnson M D 1993 *Phys. Rev. Lett.* **71** 3194
[80] Ruan W Y, Liu Y Y, Bao C G and Zhang Z O 1995 *Phys. Rev.* B **51** 7942
[81] Seki T, Kuramoto Y and Nishino T 1996 *J. Phys. Soc. Japan* **65** 3945
[82] Bao C G, Ruan W Y and Liu Y Y 1996 *Phys. Rev.* B **53** 10 820
[83] Maksym P A 1996 *Phys. Rev.* B **53** 10 871
[84] Maksym P A 1995 *Europhys. Lett.* **31** 405
[85] Bolton F and Rössler U 1993 *Superlatt. Microstruct.* **13** 139
[86] Beenakker C W J and Rejaei B 1993 *Physica* B **189** 147
[87] Jain J K and Kawamura T 1995 *Europhys. Lett.* **29** 321
[88] Heinonen O (ed) 1998 *Composite Fermions* (Singapore: World Scientific)
[89] Ruan W Y and Cheung Ho-Fai 1999 *J. Phys.: Condens. Matter* **11** 435
[90] Nazarov Yu V and Khaetskii A 1994 *Phys. Rev.* B **49** 5077
[91] Taut M 1995 *J. Phys. A: Math. Gen.* **28** 2081
[92] El Said M 1995 *Semicond. Sci. Tech.* **10** 1310
[93] Dineykhan M and Nazmitdinov R G 1997 *Phys. Rev.* B **55** 13 707
[94] Zhu J L, Li Z Q, Yu J Z, Ohno K and Kawazoe Y 1997 *Phys. Rev.* B **55** 15 819
[95] Wilson E B Jr, Decius J C and Cross P C 1955 *Molecular Vibrations* (New York: McGraw-Hill)
[96] Littlejohn R G and Reinsch M 1997 *Rev. Mod. Phys.* **69** 213
[97] Kemble E C 1937 *The Fundamental Principles of Quantum Mechanics* (New York: McGraw-Hill)
[98] Whittaker E T 1952 *Analytical Dynamics* (Cambridge: Cambridge University Press)
[99] Siegel C L and Moser J K 1971 *Lectures on Celestial Mechanics* (Berlin: Springer)
[100] Bedanov V M and Peeters F M 1994 *Phys. Rev.* B **49** 2667
[101] Schweigert V A and Peeters F M 1995 *Phys. Rev.* B **51** 7700
[102] Koulakov A A and Shklovskii B I 1998 *Phys. Rev.* B **57** 2352
[103] Date G, Murthy M V N and Vathsan R 1998 *J. Phys.: Condens. Matter* **10** 5875
[104] Imamura H, Maksym P A and Aoki H 1998 *Physica* B **249** 214
[105] Imamura H, Maksym P A and Aoki H 1998 *Phys. Rev.* B **57** R4257
[106] Kamimura H and Aoki H 1989 *Physics of Interacting Electrons in Disordered Systems* (Oxford: Oxford University Press) p 117
[107] Oguchi T and Kitatani H 1989 *J. Phys. Soc. Japan* **58** 1403
[108] Saito R 1990 *J. Phys. Soc. Japan* **59** 482
[109] Saito R and Kusakabe K 1991 *J. Phys. Soc. Japan* **60** 2388
[110] Johnson N F and Quiroga L 1997 *J. Phys.: Condens. Matter* **9** 5889
[111] Maksym P A 1997 *High Magnetic Fields in the Physics of Semiconductors II* ed G Landwehr and W Ossau (Singapore: World Scientific)
[112] Chakraborty T, Halonen V and Pietiläinen P 1991 *Phys. Rev.* B **43** 14 289

[113] Palacios J J and Hawrylak P 1995 *Phys. Rev.* B **51** 1769
[114] Benjamin S C and Johnson N F 1995 *Phys. Rev.* B **51** 14 733
[115] Bollweg K, Kurth T, Heitmann D, Vasiliadou E, Grambow P and Eberl K 1996 *Surf. Sci.* **361/2** 766
[116] Imamura H, Maksym P A and Aoki H 1996 *Phys. Rev.* B **53** 12 613
[117] Maksym P A, Imamura H and Aoki H 1996 *Proc. 23rd Int. Conf. on the Physics of Semiconductors* ed M Scheffer and R Zimmermann (Singapore: World Scientific)
[118] Partoens B, Matulis A and Peeters F M 1999 *Phys. Rev.* B **59** 1617
[119] Imamura H, Maksym P A and Aoki H 1999 *Phys. Rev.* B **59** 5817
[120] Partoens B, Schweigert V A and Peeters F M 1997 *Phys. Rev. Lett.* **79** 3990
[121] Peeters F M, Partoens B, Schweigert V A and Goldoni G 1997 *Physica* E **1** 219
[122] Partoens B, Matulis A and Peeters F M 1998 *Phys. Rev.* **57** 13 039
[123] Maksym P A, unpublished
[124] Maksym P A, unpublished
[125] Goldstein H 1980 *Classical Mechanics* (Reading, MA: Addison-Wesley)